

Magnetic excitations in pure, lightly doped, and weakly metallic La_2CuO_4

B. Keimer,* N. Belk, R. J. Birgeneau, A. Cassanho, C. Y. Chen, M. Greven, and M. A. Kastner
Center for Materials Science and Engineering, Massachusetts Institute of Technology, Cambridge, Massachusetts 02139

A. Aharony

School of Physics and Astronomy, Tel Aviv University, Tel Aviv 69978, Israel

Y. Endoh

Department of Physics, Tohoku University, Sendai 980, Japan

R. W. Erwin

National Institute of Standards and Technology, Gaithersburg, Maryland 20899

G. Shirane

Brookhaven National Laboratory, Upton, New York 11973

(Received 8 April 1992)

We report a comprehensive neutron-scattering study of the evolution of the magnetic excitations in $\text{La}_{2-x}\text{Sr}_x\text{CuO}_4$ for $0 \leq x \leq 0.04$. We first present accurate measurements of the magnetic correlation length and the sublattice magnetization of a carrier-free La_2CuO_4 crystal and analyze these in the context of recent theoretical predictions. We then systematically investigate the influence of different dopants on the magnetism: Our measurements indicate that static vacancies in the $\text{La}_2\text{Cu}_{1-y}\text{Zn}_y\text{O}_4$ system affect the magnetic correlations in a similar manner as electrons in $\text{Pr}_{2-x}\text{Ce}_x\text{CuO}_4$. The magnetic correlation length is much more rapidly suppressed as a function of x in $\text{La}_{2-x}\text{Sr}_x\text{CuO}_4$, and for $x \leq 0.04$ we find that it obeys the empirical relation $\xi^{-1}(x, T) = \xi^{-1}(x, 0) + \xi^{-1}(0, T)$, where $\xi(0, T)$ is the measured correlation length of the carrier-free sample. We also report an extensive set of measurements of the dynamical magnetic response function of a crystal of composition $\text{La}_{1.96}\text{Sr}_{0.04}\text{CuO}_4$ for excitation energies $0.75 \leq \omega \leq 45$ meV and temperatures $1.5 \leq T \leq 500$ K. The dc conductivity of this crystal exhibits three different regimes: metallic for $T \geq 100$ K, weakly localized for $100 \geq T \geq 10$ K, and strongly localized below ~ 1 K. Our neutron measurements show that the generalized susceptibility of this sample follows a surprisingly simple scaling function in the variable ω/T . This observation allows us to relate our data to a variety of normal-state properties of the layered copper oxides, in particular the dc and ac conductivities. Finally, at temperatures below ~ 20 K a "central peak" with a characteristic energy scale of less than 0.1 meV becomes prominent. Its relation to the localization of the charge carriers at low temperatures remains speculative.

I. INTRODUCTION

More than five years after the discovery of high-temperature superconductivity¹ the nature of the normal state of the copper-oxide superconductors remains an intriguing and controversial issue. While band-structure calculations succeed in predicting some features of this unusual electronic state,² it is clear that electron correlations play an important role in determining the physical properties of these compounds. As a manifestation of these correlations, magnetic fluctuations have now been detected in neutron-scattering experiments on the highest- T_c superconductors of both the $\text{La}_{2-x}\text{Sr}_x\text{CuO}_4$ (Ref. 3) and the $\text{YBa}_2\text{Cu}_3\text{O}_{6+x}$ (Ref. 4) families. However, at doping levels that give rise to superconductivity, the neutron-scattering experiments are very difficult to perform, so that our knowledge about the details of the temperature and doping dependence of the magnetic cross section in the heavily doped materials is still quite incomplete. This makes a definitive microscopic interpretation of these experimental results difficult at this

point. On the other hand, again as a result of a series of neutron-scattering measurements,^{5,6} the magnetism in the undoped parent compounds of both families is now quite well understood: Here, the system of interacting localized Cu^{2+} spins is well described by the two-dimensional (2D) Heisenberg Hamiltonian, and a small coupling between the CuO_2 layers leads to the formation of a three-dimensional Néel-ordered state. It is therefore clearly of great interest to investigate in detail the crossover from the rather conventional local moment system at zero doping to the electronic state that forms the basis for high-temperature superconductivity. While one may, in principle, expect very complicated behavior in this transition region, we will show in this article that many features of the magnetic correlations at intermediate doping levels are actually amenable to a surprisingly simple phenomenological description.

In $\text{YBa}_2\text{Cu}_3\text{O}_{6+x}$ the crossover between long-range antiferromagnetism and high-temperature superconductivity happens very rapidly around $x \approx 0.5$ due to a change in crystal structure which leads to a sudden proliferation

in the number of carriers in the CuO_2 planes. In $\text{La}_{2-x}\text{Sr}_x\text{CuO}_4$ the situation is more favorable: As shown in Fig. 1, magnetic long-range order disappears at a Sr concentration of $x \sim 0.015$, but the material becomes superconducting only above $x \sim 0.05$. The disappearance of Néel order coincides with a drastic change in the two-dimensional transport properties. The charge carriers in samples that exhibit Néel order are strongly localized, and the electronic conduction is closely similar to that of conventional lightly doped semiconductors.^{7,8} Localization effects, heralded by a decreasing conductivity as the temperature is lowered, are still apparent for samples with $0.015 \leq x \leq 0.05$ at low temperatures ($T \leq 100$ K). However, for $T \geq 100$ K the samples in this concentration regime exhibit electronic properties closely akin to the normal-state properties of the highest- T_c copper-oxide superconductors. In particular, the characteristic linear resistivity is already present for $x = 0.02$ with an amplitude, normalized to carrier concentration, almost identical to that of $\text{YBa}_2\text{Cu}_3\text{O}_7$.⁷ This, together with the relatively large magnetic correlation length, which greatly facilitates the neutron experiments, makes the transition regime $0.015 \leq x \leq 0.05$ an ideal testing ground for the role of magnetic fluctuations in the normal state of the copper-oxide superconductors. Based on a specific microscopic model, Aharony *et al.*⁹ predicted that the spin system in this concentration regime would exhibit canonical spin-glass behavior. Recent experiments¹⁰ have supported this prediction. Hence, this concentration regime

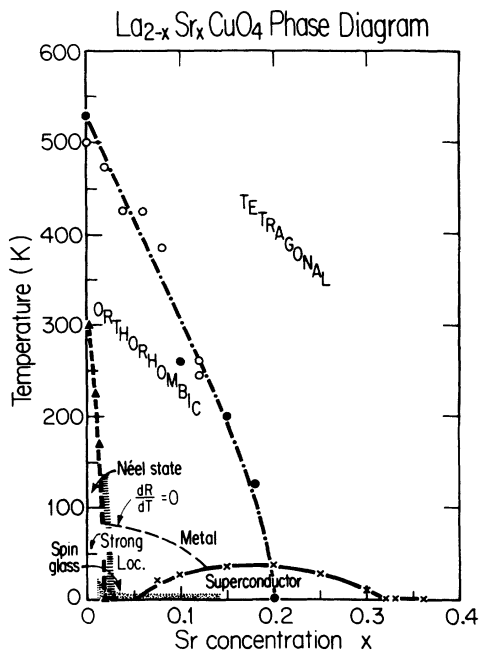


FIG. 1. Phase diagram for $\text{La}_{2-x}\text{Sr}_x\text{CuO}_4$ summarizing structural, magnetic, and transport properties. The narrow dashed line ($dR/dT=0$) separates the region of metallic linear resistance from that of logarithmically increasing resistance. The conductance in the Néel state is strongly localized. The nature and the extent of the “spin-glass” phase require further investigation.

is often referred to as the spin-glass regime. However, in the course of this article we will show that many features of the low-temperature magnetic state in this regime are closely similar to the long-range-ordered state at $x = 0$. The nature and the extent of the “spin-glass” phase boundary of Fig. 1 therefore require further investigation.

Here we report the results of a comprehensive study of the evolution of the magnetic correlations from carrier-free La_2CuO_4 well into the “spin-glass” regime. In the course of this study we have performed elastic, energy-integrating, and inelastic-neutron-scattering experiments. Most of the experiments, including all of the energy-integrating measurements, were conducted at the research reactor of the National Institute of Standards and Technology (NIST). Additional experiments to complete the empirical description were carried out at the High Flux Beam Reactor at Brookhaven National Laboratory. Our general program in this work is as follows. Based on accurate measurements of the magnetic correlation length and the sublattice magnetization of a carrier-free La_2CuO_4 sample, we first refine our understanding of the magnetic fluctuations of the Cu^{2+} spin system unaffected by doping. We then investigate the effects of both static vacancies in the $\text{La}_2\text{Cu}_{1-y}\text{Zn}_y\text{O}_4$ system and mobile holes in the $\text{La}_{2-x}\text{Sr}_x\text{CuO}_4$ system on the spin correlations. The effects of magnetic dilution via the replacement of Cu^{2+} by Zn^{2+} are surprisingly similar to those of electron doping in the $(\text{Pr,Nd})_{2-x}\text{Ce}_x\text{CuO}_4$ compounds; further we find that a percolation picture seems capable of explaining all of our data. By contrast, the effects of hole doping are genuinely novel: We first show that a temperature-independent length scale is introduced into the system. At least for $x \leq 0.04$ in $\text{La}_{2-x}\text{Sr}_x\text{CuO}_4$, the inverse magnetic correlation length is simply the sum of the inverse length scale for the doped system at $T=0$ and the inverse correlation length of the pure system: $\kappa(x, T) = \kappa(x, 0) + \kappa(0, T)$, where $\kappa(x, T)$ is the inverse magnetic correlation length. This crossover relation is inconsistent with many models that have been proposed to describe the magnetism in the disordered state.

In a recent work,¹¹ we have reported the discovery of a simple scaling relation in the dynamic response function of $\text{La}_{1.96}\text{Sr}_{0.04}\text{CuO}_4$: If plotted as a function of the scaling variable ω/T , all inelastic scattering data when normalized to their $T=0$ amplitudes collapse onto a single universal curve. We have now investigated this remarkable effect over a much wider range of excitation energies ($0.75 \leq \omega \leq 45$ meV). The previously determined simple scaling function gives an excellent overall description of the data set for $2 \leq \omega \leq 45$ meV and $1.5 \leq T \leq 500$ K with data which span a range of almost three decades in ω/T (units $\hbar = k_B = 1$). Below $\omega \sim 2$ meV and for temperatures below ~ 20 K residual effects of the spin XY anisotropy become apparent. Simultaneously a central peak with an intrinsic energy scale of less than 0.1 meV appears in the spectrum. A connection between this central peak and the spin distortion created by the carriers, which are already quite localized at these temperatures, remains speculative at the present time.

At the end of this work we will demonstrate that scattering of charged quasiparticles from the spin fluctua-

tions characterized in our experiments provides a natural explanation for some of the unusual features observed in the dc and the ac conductivities in these materials. A viable microscopic model for the unusual metallic state of these materials is still lacking, but the completeness and accuracy of the experimental investigation reported here provide a much improved basis for the construction of a proper theory.

II. SINGLE-CRYSTAL GROWTH AND CHARACTERIZATION

Large, high-quality single crystals are needed in order to perform neutron-scattering experiments on the magnetic excitations in layered copper oxides. The crystals used for the present work were grown in the Crystal Growth Central Facility at MIT. A top-seeded solution growth technique, similar to the one described in previous publications,¹² was employed to grow samples of typical volumes of $\sim 1 \text{ cm}^3$. We determined the elemental compositions of our samples by electron-probe microanalysis. We estimate the combined systematic and statistical errors to be less than ~ 0.005 for x in $\text{La}_{2-x}\text{Sr}_x\text{CuO}_4$. The scanning capability of the electron microprobe allowed us to determine the homogeneity of the Sr distribution. For each sample, the electron beam was focused on at least five different spots on the polished surface. Typically, the elemental analyses for each of these spots were well within the instrumental resolution.

Even more sensitive tests of the sample homogeneity are derived from careful studies of the sharpness of the structural and magnetic phase transitions with neutron scattering. Neutron scattering is a bulk probe, so that the entire sample volume is studied simultaneously. In pure La_2CuO_4 , a transition from a high-temperature tetragonal to a low-temperature orthorhombic phase takes place at about 520 K. This transition has been studied extensively, and the transition temperature is known to depend drastically on the concentration of strontium and oxygen dopants. Further, this transition shows true critical rather than mean-field behavior so that the transition is sensitive to any astatistical inhomogeneities on microscopic length scales of a few lattice constants. For consistency with previous work^{3,5,6} we will use the notation pertaining to the space group $Cmca$ to label the reciprocal lattice throughout this paper: In this notation the b -axis points perpendicular to the CuO_2 sheets, and the in-plane and out-of-plane reciprocal-lattice vectors have lengths 1.17 and 0.48 \AA^{-1} , respectively. Figure 2 illustrates this convention. In Fig. 3 we show the temperature dependence of the (021) superlattice reflection, which is characteristic of the low-temperature orthorhombic phase, for two of our samples. Although the structural transition temperature is depressed by about 20 K per percent Sr concentration, the order-parameter curves are perfectly sharp on a 5-K scale and they show the same critical behavior as pure La_2CuO_4 . Since any spread in the Sr or O concentrations would be reflected in a spread of transition temperatures, we conclude, in agreement with the microprobe analysis, that our samples are highly homogeneous.

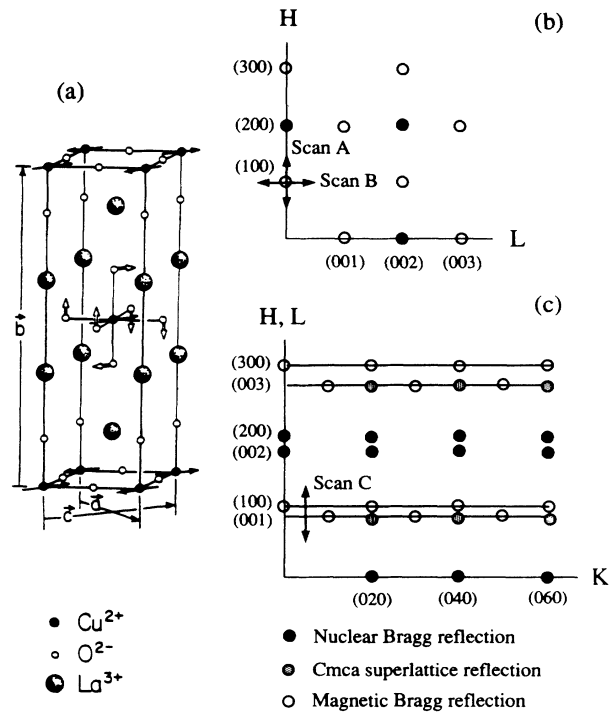


FIG. 2. (a) Unit cell of $\text{La}_{2-x}\text{Sr}_x\text{CuO}_4$ showing the spin structure in the Néel state. (b) Diagram of the in-plane reciprocal lattice [“(HOL) zone”] with nuclear and magnetic Bragg peaks. (c) Diagram of the reciprocal lattice [“(HK0) zone”], showing nuclear Bragg peaks, magnetic Bragg peaks, and the rods of 2D excitations. The shaded peaks are nuclear Bragg peaks that only exist in the low-temperature orthorhombic ($Cmca$) phase.

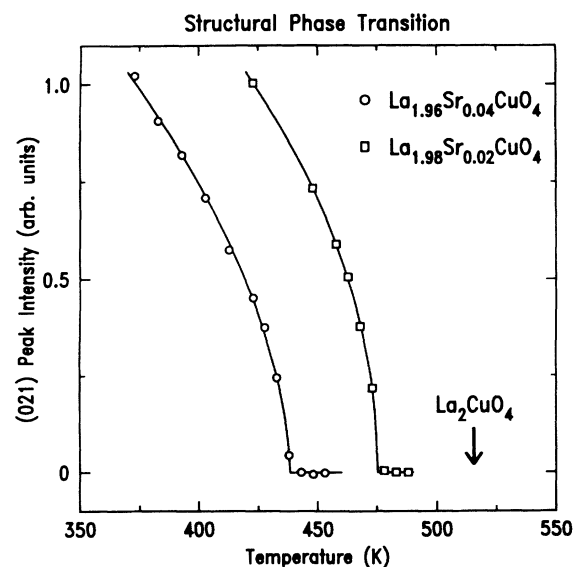


FIG. 3. Temperature dependence of the (021) nuclear reflection of two $\text{La}_{2-x}\text{Sr}_x\text{CuO}_4$ samples.

As-grown crystals of the La_2CuO_4 structure are known to contain a small amount of excess oxygen in interstitial sites. These defects introduce charge carriers into the CuO_2 planes which depress the Néel temperature and the magnetic correlation length significantly. The in-plane diffusion coefficient is very large ($\sim 10^{-14}$ cm^2/sec at room temperature¹³), so that these defects distribute homogeneously over the sample; this is confirmed by the sharp structural transitions we observe as mentioned above. Since oxygen effusion out of the sample is, however, limited by an activated surface reaction, high-temperature anneals are needed to vary the oxygen content of a given sample. We annealed several as-grown pure and doped samples for $\frac{1}{2}$ h at 900°C in vacuum ($\sim 10^{-6}$ Torr). After this procedure, a pure sample showed a Néel temperature of 325 K, identical to the highest T_N yet achieved for La_2CuO_4 ceramics. Transport measurements show that a decreased Néel temperature corresponds to a higher carrier concentration in the CuO_2 planes.⁷ We therefore assume that all oxygen acceptors have been removed from this sample. Likewise, for the doped samples we assume that all excess holes donated by oxygen impurities are removed by this technique.

III. TRANSPORT MEASUREMENTS

In the Introduction we have discussed the phase diagram of $\text{La}_{2-x}\text{Sr}_x\text{CuO}_4$, including the evolution of the transport properties as a function of the charge carrier concentration. Here we will focus on the resistivity of the $\text{La}_{1.96}\text{Sr}_{0.04}\text{CuO}_{4+\delta}$ crystal which we investigated most extensively by neutron scattering. The measurement was performed on a flawless, oriented parallelepiped of dimensions $1.5 \times 2 \times 1.2$ mm^3 cut from the $\sim 1\text{-cm}^3$ crystal. This sample was etched for 15 min in a solution of 2% bromine in methanol and then ultrasonically cleaned in acetone and methanol. A standard four-probe silver contact configuration was evaporated onto a b-oriented surface of the sample, and an ultrasonic wire bonder was used to attach gold leads to the sample contacts. The sample was mounted in a helium flow inside a cryostat for temperatures above 2 K and in a dilution refrigerator for lower temperatures. The data were taken using a lock-in amplifier at 28 Hz and ac bias currents beneath the levels at which sample heating was induced.

The top panel of Fig. 4 shows the in-plane resistivity as a function of temperature thus obtained. The data are nearly identical to those reported by Preyer *et al.*⁷ for a $\text{La}_{1.98}\text{Sr}_{0.02}\text{CuO}_{4+\delta}$ sample, despite the lower Sr concentration of the latter. Presumably this is offset by a higher oxygen concentration. As pointed out by Preyer *et al.*,⁷ the slope of the resistivity gives a scattering rate of order T , the same as found in the normal state of the highest- T_c superconductors. The dependence of the conductance on temperature is logarithmic between ~ 100 and ~ 10 K. This is illustrated in the middle panel of Fig. 4, where the 2D conductivity, the conductance per square per CuO_2 layer, is plotted versus $\log_{10}T$. At lower temperatures, however, the temperature dependence becomes exponential. In the bottom panel of Fig. 4 the logarithm of the

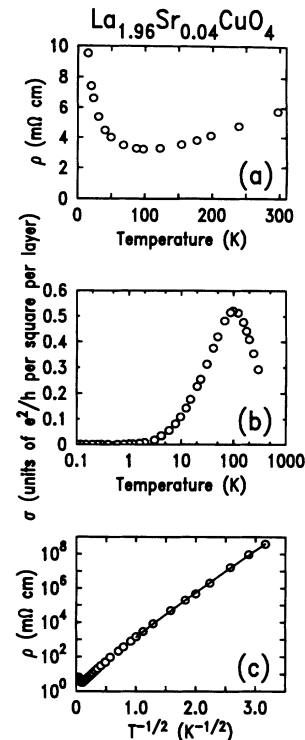


FIG. 4. (a) In-plane resistivity of a $\text{La}_{1.96}\text{Sr}_{0.04}\text{CuO}_4$ crystal. (b) Two-dimensional conductance per square per CuO_2 layer, plotted vs $\log_{10}T$. (c) Low-temperature in-plane resistivity, plotted such that the functional dependence $\rho \sim e^{(T_{\text{CG}}/T)^{1/2}}$ is highlighted. The solid line represents a fit to this form, as discussed in the text.

resistivity is plotted as a function of $T^{-1/2}$ to show that the resistivity follows $\exp[(T_{\text{CG}}/T)^{1/2}]$ from ~ 1 to ~ 0.1 K. A least-squares fit of the data to the form $\exp[(T_{\text{CG}}/T)^\nu]$ gives $\nu = 0.5 \pm 0.05$ and $T_{\text{CG}} = 50$ K. The crossover between the logarithmic and exponential behavior occurs between ~ 10 and ~ 1 K.

The high-temperature behavior of the resistivity is well described by the simple form

$$R_{\text{square}} = (l^{-1} + L_{\text{in}}^{-1}) \frac{h}{e^2 k_F}, \quad (1)$$

where l and L_{in} are the elastic and inelastic scattering lengths, respectively, and k_F is the Fermi wave vector. Fitting the linear T dependence in Fig. 4(a) gives $L_{\text{in}} = l \times 100$ K/T. At $T=0$, $L_{\text{in}}^{-1} = 0$ and we find from Fig. 4(a) $k_F l \approx 1$. The value of $k_F \approx 10^{-1} \text{ \AA}^{-1}$ computed from the Sr concentration yields $l \approx 10$ \AA , and, thence, $L_{\text{in}} \approx 1000$ \AA K/T.

Relation (1) holds at high T , but at lower T , as $L_{\text{in}} > l$, the logarithmic corrections to the conductance become apparent. The simplest interpretation is that the latter corrections arise from weak localization. However, the magnetoresistance results of Preyer *et al.*,¹⁴ who find an isotropic negative magnetoresistance, suggest that the onset of localization is quite unconventional. At still lower temperatures the temperature dependence becomes ex-

ponential, signaling the crossover to strong localization. This occurs when L_{in} becomes larger than the localization length λ . Using $L_{\text{in}} \approx 1000 \text{ \AA} \text{ K}/T$ from the high-temperature resistivity and the crossover temperature $\sim 10 \text{ K}$, one finds $\lambda \approx 100 \text{ \AA}$. Since this is larger than the magnetic correlation length in this sample we would expect that localization would have little effect on the dynamic magnetic response. As we will see in Sec. IX of this article, our neutron-scattering measurements are consistent with this expectation.

The most straightforward explanation of the $\exp[(T_{\text{CG}}/T)^{-1/2}]$ dependence is that it arises from variable-range hopping in a Coulomb gap, as explained by Efros and Shklovskii.¹⁵ The energy scale of this correlation-limited hopping, T_{CG} , is determined by the Coulomb interaction of two electrons separated by the localization length. Although we have not measured the temperature dependence of the anisotropy of the hopping conductivity, we expect it to become three dimensional at low T , as Preyer *et al.*⁷ found for lightly doped $\text{La}_2\text{CuO}_{4+\delta}$. For the 3D case Efros and Shklovskii¹⁵ give $T_{\text{CG}} = 2.8e^2/\epsilon\lambda$, where ϵ is the dielectric constant which, with $\lambda = 100 \text{ \AA}$, gives $\epsilon = 90$. This value represents a three-dimensional average over a highly anisotropic dielectric tensor. Assuming that $\epsilon = (\epsilon_a^2 \epsilon_b)^{1/3}$, and using the value for the dielectric constant in the b direction $\epsilon_b = 27$ measured by Chen *et al.*,⁸ one finds the value for the in-plane (a) direction to be $\epsilon_a \sim 160$. Chen *et al.*⁸ found values of more than 100 at hole concentrations $x \sim 0.007$, and we would have expected ϵ_a to grow rapidly with concentration. However, given the experimental uncertainties in the various measured quantities and the highly simplified treatment of the anisotropy we consider the overall consistency with Chen *et al.*⁸ to be quite satisfactory.

The Coulomb gap influences hopping only at temperatures low enough that the typical energy for a hop is less than the Coulomb gap. Efros and Shklovskii¹⁵ show that the crossover temperature from $\exp[(T_{\text{CG}}/T)^{1/2}]$ to $\exp[(T_0/T)^{1/4}]$ increases with $N_0(E_F)$, the density of states at the Fermi energy. This happens because the Coulomb gap increases with $N_0(E_F)$ and, in addition, because the average hopping energy decreases with $N_0(E_F)$. Thus, many doped semiconductors are found to follow the $\exp[(T_{\text{CG}}/T)^{1/2}]$ dependence close to the insulator-to-metal transition, where the density of states is high. Using the analysis of Efros and Shklovskii one expects the transition for the sample of Fig. 4 to occur above $\sim 12 \text{ K}$. Because this is in the crossover regime between strong and weak localization, the conventional hopping is not seen. In much more lightly doped samples the $T^{1/4}$ hopping is, indeed, observed.⁷

IV. MAGNETIC NEUTRON SCATTERING

Since we have utilized magnetic neutron scattering extensively to investigate our samples, it will prove useful to review some basic properties of the cross section for magnetic neutron scattering in the context of the copper-oxide materials. The cross section measured in a magnetic neutron-scattering experiment is related to the pair

correlation function between spins according to the relation

$$\frac{d^2\sigma}{d\Omega dE_f} \sim f^2(\mathbf{Q}) \frac{k_f}{k_i} \sum_{\alpha\beta} (\delta_{\alpha\beta} - \hat{Q}_\alpha \hat{Q}_\beta) S^{\alpha\beta}(\mathbf{Q}, \omega), \quad (2)$$

where the ‘‘dynamical structure factor’’ is defined as

$$S^{\alpha\beta}(\mathbf{Q}, \omega) = \frac{1}{2\pi} \sum_1 \int_0^\infty dt e^{i(\mathbf{Q}\cdot\mathbf{1} - \omega t)} \langle S^\alpha(0,0) S^\beta(\mathbf{1}, t) \rangle. \quad (3)$$

The energies and wave vectors of the incoming and scattered neutrons are denoted by E_i , E_f , \mathbf{k}_i , and \mathbf{k}_f , respectively, and we adopt the notation $\omega = E_f - E_i$ and $\mathbf{Q} = \mathbf{k}_f - \mathbf{k}_i$. The magnetic form factor $f(\mathbf{Q})$ of Cu^{2+} in La_2CuO_4 has been found¹⁶ to be rather weakly \mathbf{Q} dependent below $|\mathbf{Q}| \leq 2 \text{ \AA}^{-1}$, where most of our experiments were done.

In an isotropic spin system with antiferromagnetic correlations, the cross section for inelastic magnetic scattering is simply proportional to the dynamical structure factor $S(\mathbf{Q}, \omega)$. For a two-dimensionally correlated system such as doped La_2CuO_4 , $S(\mathbf{Q}, \omega)$ is independent of the momentum transfer Q_b perpendicular to the CuO_2 layers, so that each magnetic reciprocal-lattice point is the origin of a rod of 2D inelastic scattering extending in the b direction.

With a triple-axis spectrometer one can only access the region near a particular plane of reciprocal space without remounting the crystal, so that two different scattering geometries have to be distinguished: First, if the 2D excitation rod is oriented perpendicular to the scattering plane, all momentum transfers of the form (HOL) can be reached [Fig. 2(b)]. In this configuration the full geometry of $S(\mathbf{Q}, \omega)$ within the CuO_2 layers can be measured. However, kinematical constraints as well as contamination from double scattering events at the elastic (100) position and from the unscattered beam restrict the range of energy transfers for high-quality inelastic experiments to $4.5 \leq \omega \leq 12 \text{ meV}$. In order to extend the dynamic range of our measurements to lower and higher energy transfers, we remounted our sample to orient the 2D rod into the scattering plane, so that momentum transfers of the form ($HK0$) became accessible [Fig. 2(c)]. In this geometry, the restrictions limiting the range of energy transfers can be overcome by systematically varying the momentum transfer K perpendicular to the CuO_2 layers.

The quantity usually predicted by theory is the generalized susceptibility $\chi(\mathbf{Q}, \omega)$, whose imaginary part is related to the dynamical structure factor according to

$$S(\mathbf{Q}, \omega) = \frac{1}{1 - \exp(-\omega/T)} \chi''(\mathbf{Q}, \omega). \quad (4)$$

The \mathbf{Q} dependence of the zero-frequency limit of the generalized susceptibility, $\chi(\mathbf{Q}) = \chi(\mathbf{Q}, \omega = 0)$, provides information about the spatial range of the magnetic correlations. Although a measurement of the temperature and doping dependence of the magnetic correlation length is clearly of great interest, an exact experimental determination of $\chi(\mathbf{Q})$ would be extremely difficult, since it is relat-

ed to the experimentally accessible $S(\mathbf{Q}, \omega)$ by a variant of the Kramers-Kronig transformation

$$\chi(\mathbf{Q}) = \frac{1}{T} \int_{-\infty}^{\infty} d\omega \frac{1 - e^{-\omega/T}}{\omega/T} S(\mathbf{Q}, \omega). \quad (5)$$

In principle, therefore, one would have to measure the entire dynamic response function of the system in order to determine the magnetic correlation length. We have circumvented this difficulty by using an experimental trick originally discovered by Birgeneau, Skalyo, and Shirane¹⁷ to determine a good approximation to the instantaneous correlation function

$$\begin{aligned} S(\mathbf{Q}) &= \frac{1}{N} \langle S(-\mathbf{Q}, 0) S(\mathbf{Q}, 0) \rangle = \int_{-\infty}^{\infty} d\omega S(\mathbf{Q}, \omega) \\ &\approx \int_{-T}^{E_l} d\omega S(\mathbf{Q}, \omega). \end{aligned} \quad (6)$$

As discussed in detail in previous publications,^{5,6} this quantity is measured by removing the analyzer from the triple-axis spectrometer and orienting the sample such that the wave vectors of the scattered neutrons are parallel to the 2D rod. For an incident neutron energy of 30.5 meV, this condition is satisfied at the point (1, 0.38, 0) in reciprocal-lattice units.

The detailed balance factor in Eq. (5) and the incident neutron energy introduce effective cutoffs into the energy integration. If these are larger than typical fluctuation energies of the spin system, the integration is properly carried out and the magnetic correlation length can be extracted from the data without further corrections. If the cutoff energy is of the same order as the characteristic energy scale of the spin system, the correlation length obtained by this method may deviate somewhat from the intrinsic magnetic correlation length. In La_2CuO_4 , where a full theory for $S(\mathbf{Q}, \omega)$ exists, one can estimate the error introduced by the cutoffs by using Eq. (5) and the theoretical $S(\mathbf{Q}, \omega)$. As we will discuss in the next section, we have performed such a calculation and found the error to be negligible over most of the temperature range covered by our experiments.

V. CARRIER-FREE La_2CuO_4

After the discovery of high-temperature superconductivity there was considerable debate about the magnetic ground state of the undoped cuprate materials: spin-density waves and exotic quantum states were among the possible candidates. The experiments of Vaknin *et al.*¹⁸ who discovered an ordered moment close to the value calculated from spin-wave theory in La_2CuO_4 , and Endoh *et al.*,⁵ who found a strongly diverging magnetic correlation length as the temperature was lowered toward the Néel temperature from above, showed convincingly that La_2CuO_4 is a local moment Heisenberg antiferromagnet whose only unusual feature is the low spin quantum number $S = \frac{1}{2}$. Chakravarty, Halperin, and Nelson¹⁹ succeeded in calculating the temperature dependence of the magnetic correlation length of the spin- $\frac{1}{2}$ Heisenberg antiferromagnet, and they obtained to first order

$$\xi = 0.24 \frac{c}{2\pi\rho_s} \exp \left[\frac{2\pi\rho_s}{T} \right], \quad (7)$$

where c is the spin-wave velocity and $2\pi\rho_s$ is the spin stiffness constant. $c = 850 \text{ meV}\text{\AA}$, corresponding to a nearest-neighbor (NN) superexchange $J \sim 135 \text{ meV}$, has been measured by high-energy neutron scattering²⁰ and two-magnon light scattering.²¹ The calculation of Ref. 19 was based on a renormalization-group analysis of the quantum nonlinear σ model (QNL σ M), which was argued to be the appropriate continuum limit of the quantum Heisenberg model. As a function of its coupling constant g , the QNL σ M exhibits a phase transition from a regime in which its ground state is Néel ordered at $T=0$ into a region in which quantum fluctuations are sufficiently strong to disorder the system even at zero temperature. It was argued that even for $S = \frac{1}{2}$, g was small enough for a transition to antiferromagnetic (AF) long-range order to occur at $T=0$. In this regime, the quantum spin system can be mapped onto its corresponding classical one. The preexponential factor in Eq. (7) was calculated approximately by matching the renormalization-group analysis with a Monte Carlo simulation of the classical 2D Heisenberg model. To within the combined experimental and theoretical errors, Eq. (7) with $2\pi\rho_s = 0.94J = 127 \text{ meV}$, obtained from spin-wave theory gave a good description of the experimental data for as-grown La_2CuO_4 .

Since then, it was realized that as-grown La_2CuO_4 contains a small number of excess charge carriers, and that even a minute amount of carriers can have a significant influence on the magnetic correlation length. Concurrently, the theoretical predictions for the magnetic correlation length also became more quantitative: Recently, an exact analytic calculation of the preexponential factor, including the first $O(T)$ correction, has become available. Hasenfratz and Niedermayer²² quote

$$\xi = \frac{e}{8} \frac{c}{2\pi\rho_s} \exp \left[\frac{2\pi\rho_s}{T} \right] \left[1 - 0.5 \frac{T}{2\pi\rho_s} \right]. \quad (8)$$

Numerical simulations of the NN spin- $\frac{1}{2}$ 2D quantum Heisenberg antiferromagnet have also improved considerably. In the most accurate quantum Monte Carlo study to date, Ding and Makivic²³ find that their numerical data are best fit by

$$\xi = 0.276a \exp \frac{1.25J}{T}. \quad (9)$$

In order to test these theoretical predictions and to create a reference point for our studies of doped La_2CuO_4 , we have measured the instantaneous correlation function for the carrier-free La_2CuO_4 sample whose preparation we described in Sec. II. The measurements were carried out at the BT9 spectrometer at NIST in the energy-integrating mode described above, with an incident neutron energy of 30.5 meV and collimations 10'-10'-10'. Representative data are shown in Fig. 5. The scans up to about 50 K above the Néel temperature of 325 K were resolution limited, but at higher temperatures we were able to extract the intrinsic peak width by fitting our data

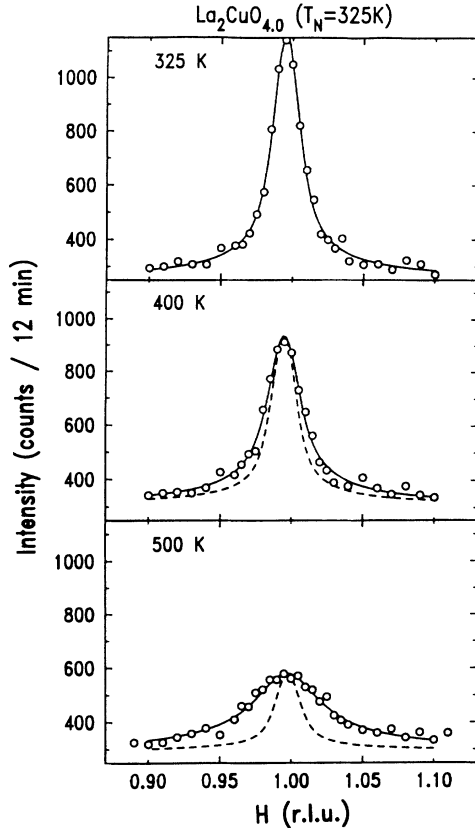


FIG. 5. Representative energy-integrating scans along $(H, 0.38, 0)$ for carrier-free La_2CuO_4 ($T_N=325$ K). The dashed line is the experimental resolution function; the solid line the result of a fit to a convolution of the resolution function with a two-dimensional Lorentzian scattering function.

to simple Lorentzians, $S(q) = S(0)/(1 + q^2\xi^2)$ convoluted with the experimental resolution function. The result of this procedure is shown in Fig. 6(a), together with the theoretical predictions Eqs. (8) and (9). Since $J \sim 135$ meV has been determined experimentally, the Monte Carlo prediction contains no adjustable parameters. For the analytical formula Eq. (8) we obtained $2\pi\rho_s = 150$ meV = $1.11J$ from a least-squares fit to our data. The agreement between the fitted curve, the Monte Carlo simulation, and our data is clearly good. For comparison, the curve calculated from Eq. (8) with the spin-wave theory value¹⁹ of $2\pi\rho_s = 0.94J$ deviates significantly from both the experimental and the numerical data. This indicates an $\sim 15\%$ error in calculating $2\pi\rho_s$ from spin-wave theory. As we will see shortly, our estimate of this error is somewhat reduced if corrections to the 2D Heisenberg Hamiltonian are taken into account. It is gratifying to see that both experiment and theory are now sufficiently far advanced that this small error is clearly noticeable.

The temperature dependence of $S(0)$, the $q=0$ instantaneous correlation function, is shown in Fig. 6(b). Up to a negligibly small $O(T)$ correction, the predictions of Chakravarty, Halperin, and Nelson¹⁹ and Tyc, Halperin, and Chakravarty²⁴ for $S(0)$ are

$$S(0) = C_S \left[\frac{T}{2\pi\rho_s} \right]^2 \xi^2. \quad (10)$$

A very similar result was obtained by Kopietz²⁵ in the Schwinger boson formalism. The constant C_S is not determined by our experiment, and in Fig. 6(b) the overall scale was adjusted in order to obtain the best fit of Eq. (10) to the data.

In order to estimate the effect of the cutoff in the energy integration on the correlation length deduced in our experiment, we have calculated the integral Eq. (5) numerically, using the dynamic structure factor of Tyc *et al.*²⁴ These authors find that the characteristic energy of the spin system is given by $\omega_0 = c\xi^{-1}[T/2\pi\rho_s]^{1/2}$. For energies up to 12 meV, this prediction has been experimentally verified by Yamada *et al.*⁶ We have fitted the data generated by a numerical integration of Eq. (5) to simple Lorentzians and thus established a conversion table between the correlation length measured in our experiment and the intrinsic correlation length. We found that the two lengths are indistinguishable over most of the temperature range. A noticeable difference, although still within the experimental error bar, only appears above 500 K. To take this discrepancy into account, we have adjusted the error bars of the highest temperature points in Fig. 6(a). The insensitivity of the measured correlation length to the cutoff is hardly surprising, since even at 600 K the characteristic frequency is still only 20

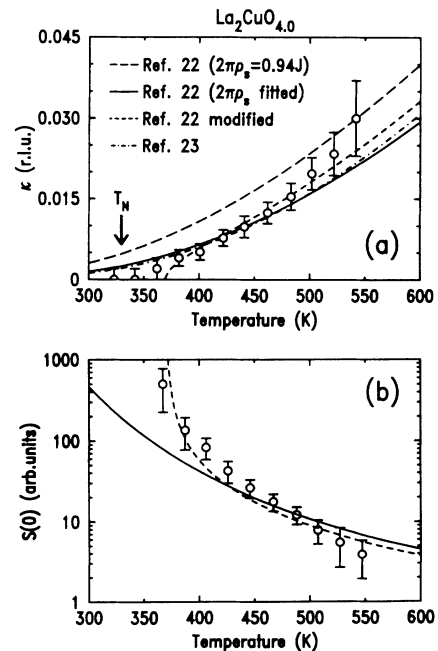


FIG. 6. (a) Inverse magnetic correlation length of a carrier-free La_2CuO_4 sample together with several theoretical predictions, as discussed in the text. (b) Peak intensities of the 2D Lorentzian fits to the energy-integrating scans for this sample. The short-dashed line in both figures refers to the expression of Hasenfratz and Niedermayer, Ref. 22, modified according to Eq. (12) in the text.

meV, significantly less than both cutoff energies. As a last crosscheck, we have also computed the integrated intensities $I = [S(0)/\xi^2] \ln(\xi/a)$ of the 2D Lorentzian fits to our experimental data. We have found that I is constant over the entire temperature range, supporting our point above: If, on heating, ω_0 increased above the cutoff frequency, the integrated intensity would be reduced. This is clearly not the case. Together, these arguments demonstrate convincingly that the magnetic correlation length is correctly determined by our measurement technique.

A close look at Figs. 6(a) and 6(b) reveals that, despite the good overall agreement, the experimentally determined quantities ξ and $S(0)$ diverge somewhat more rapidly with decreasing T than the theoretical curves. This is not surprising, since it is expected that close to the Néel temperature terms beyond those contained in the 2D Heisenberg Hamiltonian become relevant and begin to enhance the correlation length.

To a first approximation it is appropriate to neglect corrections to the 2D Heisenberg Hamiltonian due to the local orthorhombicity and the three-dimensional structure since these terms are about 4 orders of magnitude smaller than the primary energy scale. These corrections are nevertheless quite important as evidenced by the fact that the zero-temperature transition of the underlying 2D Heisenberg model is shifted to ~ 325 K in undoped La_2CuO_4 . Three types of weak perturbation to the primary Hamiltonian are responsible for the transition to three-dimensional long-range order at this relatively high temperature: Spin-orbit coupling results in an exchange anisotropy of XY symmetry and an antisymmetric exchange term which lifts the XY degeneracy, and the unfrustrated exchange between neighboring layers in the orthorhombic crystal structure leads to a small interlayer coupling. The full spin Hamiltonian for La_2CuO_4 can thus be written

$$H = J \left[\sum_{i\delta_{\parallel}} \mathbf{S}_i \cdot \mathbf{S}_{i+\delta_{\parallel}} + \alpha_{xy} \sum_{i\delta_{\parallel}} S_i^b S_{i+\delta_{\parallel}}^b + \alpha_{DM} \sum_{i\delta_{\parallel}} (S_i^b S_{i+\delta_{\parallel}}^c - S_{i+\delta_{\parallel}}^b S_i^c) + \alpha_1 \sum_{i\delta_1} \mathbf{S}_i \cdot \mathbf{S}_{i+\delta_1} \right]. \quad (11)$$

The various interaction parameters have been measured experimentally by low-energy neutron scattering and the investigation of magnetoresistive anomalies at spin reorientation transitions as discussed in Refs. 26 and 27. The effects of the antisymmetric exchange term α_{DM} are reduced by the factor $\sin\theta_T$, where θ_T is the tilt angle. In the Néel state, α_{xy} and α_{DM} introduce gaps for $\mathbf{q}=0$ spin fluctuations polarized out of plane and in plane, respectively: $\Delta E_{xy} = 2.32J\sqrt{2}\alpha_{xy} \approx 2.5$ meV and $\Delta E_{DM} = 2.32J\alpha_{DM} \approx 1$ meV were measured in a sample with a Néel temperature of 190 K.²⁸ However, the ordered Cu moment is considerably reduced in samples with reduced Néel temperatures and the spin-wave gap energies are correspondingly diminished. For the

$T_N = 325$ K sample, we have recently determined²⁹ $\Delta E_{xy} = 5.5$ meV and $\Delta E_{DM} = 2.3$ meV so that $\alpha_{xy} = 1.5 \times 10^{-4}$, $\alpha_{DM} = 7.5 \times 10^{-3}$, and $\alpha_1 = 5 \times 10^{-5}$.

Above the Néel temperature, we expect these perturbations to become relevant as $\alpha_{\text{eff}} \xi^2 \sim 1$, where $\alpha_{\text{eff}} \approx 1 \times 10^{-4}$ is a suitable combination of the perturbative terms. Because of the exponential divergence of the correlation length, the transition to Néel order takes place shortly thereafter, such that $T_N/J \approx 4\pi\rho_s / \ln(1/\alpha_{\text{eff}})$. Using $2\pi\rho_s \approx 140$ meV, this yields $T_N \approx 350$ K, quite close to the measured value of 325 K. A more detailed discussion of the Néel transition can be found in Ref. 27.

Above the Néel transition it is difficult to evaluate properly the influence of the various perturbations on the correlation length. However, in the crossover region in which the correlation length is not large enough for three-dimensional critical fluctuations to be important, one can write down a generic mean-field expression:

$$\xi(\alpha_{\text{eff}}, T) = \frac{\xi_0(T)}{\sqrt{1 - \alpha_{\text{eff}} \xi_0(T)^2}}, \quad (12)$$

where again α_{eff} is a suitable combination of the perturbative terms, and $\xi_0(T)$ denotes the correlation length of the unperturbed Heisenberg system. As mentioned above, α_{xy} and α_{DM} introduce gaps into the spin-wave spectrum. These gaps are similar to that introduced by a staggered external field. We have thus integrated the recursion relations of Chakravarty, Halperin, and Nelson¹⁹ with such a field $h \sim \alpha_{\text{eff}}$, and found that Eq. (12) holds in the classical limit to one-loop order. The treatment of α_1 is more complicated, but within reasonable approximations yields a similar limiting classical result. Because of ambiguities in the short-distance cutoff of the renormalization-group analysis and in the precise role of the various perturbations, α_{eff} is only defined up to a factor of order unity.

We have therefore varied both $2\pi\rho_s$ and α_{eff} in Eq. (12) in order to obtain the best fit to our data for the correlation length of the carrier-free La_2CuO_4 crystal. $\xi_0(T)$ was calculated from Eq. (8). The result, corresponding to $2\pi\rho_s = 140$ meV and $\alpha_{\text{eff}} = 6.5 \times 10^{-4}$, is shown in Fig. 6(a). In the light of the uncertainties in the definition of α_{eff} , the fitted value appears quite reasonable, and the agreement of the theoretical expression with the experimental data has obviously improved. Likewise, using expression (12) with the same α_{eff} in the prediction of $S(0)$, Eq. (10), improves the agreement between theory and experiment in Fig. 6(b). Although a more elaborate formula for $\xi(\alpha_{\text{eff}}, T)$ is highly desirable, it therefore appears likely that Eq. (12) is an adequate description for the correlation length not too close to the Néel temperature.

For $T \geq 500$ K, a systematic deviation from the fit, albeit within the experimental error, is still discernible. Such an effect may arise from an effective temperature dependence of ρ_s due to changes in the lattice parameters as well as thermal vibrations. There may also be additional thermal effects affecting the relationship between ρ_s and the superexchange constant J . A relatively subtle decrease of J ($\sim 10\%$ at $T = 550$ K relative to its room-

temperature value) would be sufficient to explain the remaining discrepancy. Thermally excited carriers could also play a role.

Thus, while the overall agreement between calculations based on the 2D Heisenberg antiferromagnet and our measurements is satisfactory, additions to this Hamiltonian due to the orthorhombic crystal symmetry complicate the interpretation of some quantitative details of our measurements. We have recently performed a similar experiment on $\text{Sr}_2\text{CuO}_2\text{Cl}_2$, a material which due to its tetragonality is expected to be a better realization of the 2D Heisenberg model: While α_{xy} is of similar magnitude as in La_2CuO_4 , α_{DM} vanishes and α_1 is negligibly small. The magnetic correlation length measured in this material follows the predictions of Eqs. (8) and (9) extremely well, but some differences between the measured $S(0)$ and Eq. (10) remain. We defer a discussion of the details of these studies to a forthcoming publication.³⁰

VI. DOPING EFFECTS IN THE NÉEL STATE

The preceding section shows that we have now arrived at a very detailed picture of the magnetic state of undoped La_2CuO_4 . Experimental studies of other undoped layered copper oxides have not been as exhaustive, but the differences between the compounds are in any case quite subtle. This provides a good basis for a systematic investigation of the effects of doping on the magnetic state of these materials. Dopants introduce defects into the interacting spin system. We have studied the effects of two different dopants on the magnetic state of La_2CuO_4 : Zn^{2+} , which introduces static vacancies into the spin system, and Sr^{2+} , which creates mobile holes at sufficiently large temperatures and concentrations. We also discuss previously obtained data^{5,6} on samples of $\text{La}_2\text{CuO}_{4+\delta}$ with various values of excess oxygen δ incorporated in the growth process. We first focus on the $\text{La}_2\text{Cu}_{1-y}\text{Zn}_y\text{O}_4$ system.

The Zn^{2+} ion is in a nonmagnetic $3d^{10}$ configuration and, being of the same size as Cu^{2+} , occupies the copper sites in the crystal structure. The additional electron introduced by replacing Cu^{2+} with Zn^{2+} is tightly bound to the donor site, so that the substitution is equivalent to a removal of Cu^{2+} spins from the network. We prepared a series of $\text{La}_2\text{Cu}_{1-y}\text{Zn}_y\text{O}_4$ single crystals and measured their Néel temperatures by SQUID magnetometry. We then removed all oxygen impurities from our samples by subjecting them to the annealing procedure described in Sec. II above, and remeasured their Néel temperatures. The result is shown in the left-hand panel of Fig. 7. It is clear from this figure that the effect of the interstitial oxygen impurities on T_N simply adds on to the effect of the dilution. The $T_N(y)$ curve for the crystals without oxygen impurities extrapolates to zero at $y \approx 0.26$. This value is quite close to but slightly larger than that indicated by recent measurements on powder samples.³¹ As noted in Refs. 27 and 31, the concentration of $y = 0.26$ is somewhat smaller than the nearest-neighbor site percolation threshold ($y = 0.41$). Figure 7 demonstrates a remarkable fact: The rates at which T_N is suppressed with doping are identical in the $\text{La}_2\text{Cu}_{1-y}\text{Zn}_y\text{O}_4$ and

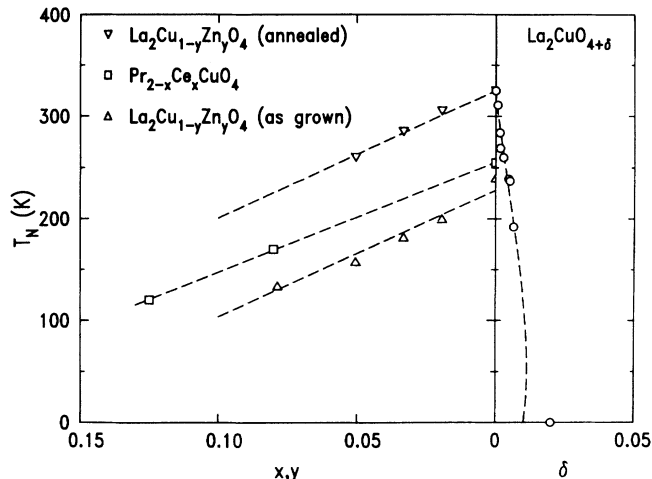


FIG. 7. Néel temperature as a function of electron and hole concentration. For the latter data from Ref. 8 the hole concentration was measured using the Hall effect.

$\text{Pr}_{2-x}\text{Ce}_x\text{CuO}_4$ systems, although the latter system is metallic at least above $x \sim 0.1$. This becomes even more surprising if one considers the symmetry of the donor sites: Each electron donated by the Ce dopants should be shared equally between four Cu sites around a plaquette, so that the magnetic state is more sensitive to Ce doping than to site dilution. Recently a model has been proposed³² to rationalize at least part of this surprising behavior: Oxygen impurities in interstitial sites may help to localize the electrons at a specific Cu site. This explains the striking similarity of the T_N suppression in $\text{La}_2\text{Cu}_{1-y}\text{Zn}_y\text{O}_4$ and $(\text{Nd},\text{Pr})_{2-x}\text{Ce}_x\text{CuO}_4$, but leaves open the question of the conduction mechanism in the latter sequence of compounds.

The right-hand panel of Fig. 7 shows that hole doping suppresses the Néel temperature much more rapidly than electron doping: About 1.5% holes are sufficient to destroy the Néel state completely. In order to explore the reason for this remarkable asymmetry, we now discuss the effects of doping on the sublattice magnetization and the magnetic correlation length.

The (100) Bragg peak intensity, normalized to the intensity at 10 K, of the carrier-free sample is shown in Fig. 8(a), together with data for La_2CuO_4 doped with various amounts of oxygen. In Ref. 27 we have shown that the temperature dependence of the sublattice magnetization in pure La_2CuO_4 is in quantitative agreement with a spin-wave analysis of the Hamiltonian (11). The temperature dependence of the sublattice magnetization for the hole-doped samples evolves continuously with dopant concentration: At low temperatures, the sublattice magnetization curve first flattens and ultimately becomes reentrant, while additional 2D diffuse scattering appears.⁵ In agreement with the model proposed by Aharony *et al.*,⁹ this indicates that, at least in the limit in which the holes are well localized, they frustrate the superexchange interaction between the Cu spins and hence lead to a rapid suppression of T_N . Similar reentrancy effects have been observed in the $\text{YBa}_2\text{Cu}_3\text{O}_{6+x}$ compound for $0.2 \leq x \leq 0.4$.³³ In this system the interpretation of these

effects is complicated by the presence of Cu moments in the chain layers. By contrast, such behavior is observed neither in the data for the diluted samples²⁷ nor in equivalent data for the $\text{Pr}_{2-x}\text{Ce}_x\text{CuO}_4$ system.²⁶ Thus, frustration is presumably not a major factor in the destruction of long-range antiferromagnetism in the compounds doped with excess electrons.

We show in Fig. 8(b) the measured inverse correlation lengths in the three $\text{La}_2\text{CuO}_{4+\delta}$ samples of Fig. 8(a) with Néel temperatures of 325, 190, and 90 K. The hole concentration varies approximately linearly with $(325 \text{ K} - T_N)$. It is evident that at very high temperatures, 500–600 K, the correlation length varies little with doping. However, the growth of the spin correlations is increasingly inhibited by the holes as the temperature is decreased. This behavior is in marked contrast with equivalent results in the electron-doped materials³² where the added electrons simply reduce ρ_s in accord with percolation.

Several authors^{34,35} have considered an extension of the quantum nonlinear σ model as a model for the destruction of Néel order in La_2CuO_4 . In a simplified picture, the main effect of doping could be to increase the quantum coupling constant g in an otherwise effective

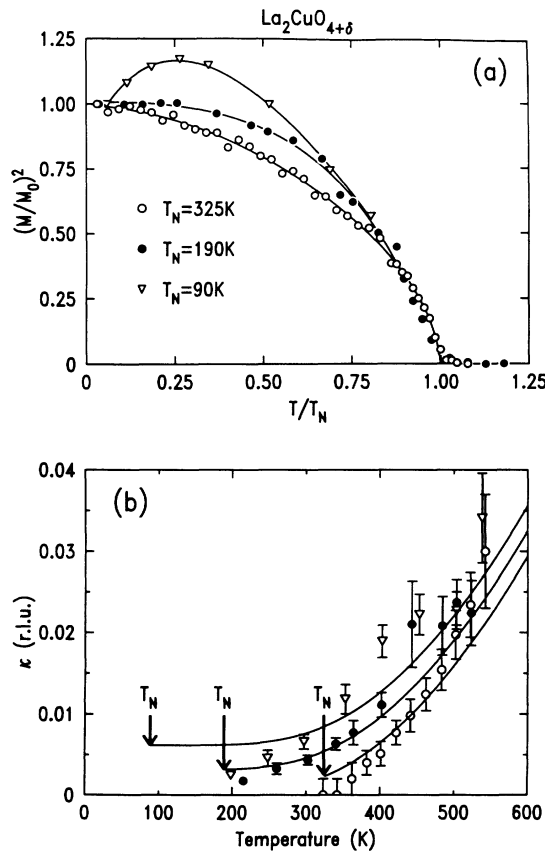


FIG. 8. (a) Square of the sublattice magnetization of undoped ($T_N = 325 \text{ K}$) and oxygen-doped ($T_N = 190$ and 90 K) samples. The solid lines are guides to the eye. The data for $\text{La}_2\text{CuO}_{4+\delta}$ are from Ref. 5. Some degree of inhomogeneity is present in the $T_N = 90\text{-K}$ sample (Ref. 5). (b) Inverse magnetic correlation length of the same samples. The solid lines are calculated from $\kappa(x, T) = \kappa(x, 0) + \kappa(0, T)$.

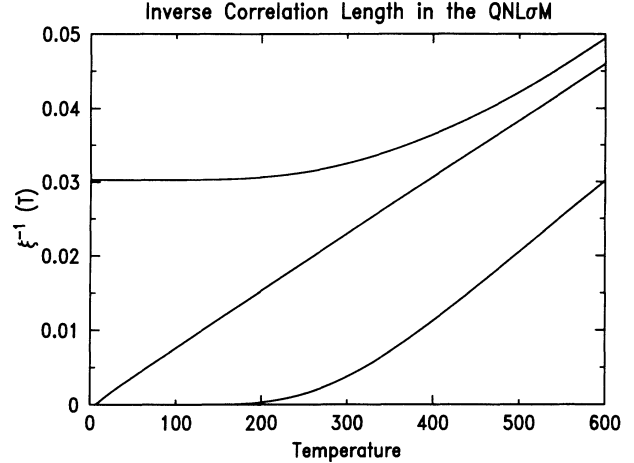


FIG. 9. Qualitative behavior of the inverse magnetic correlation length in the quantum disordered (upper curve), quantum critical (middle curve), and renormalized classical (lower curve) regimes of the quantum nonlinear σ model, as calculated from a one-loop renormalization-group analysis (Ref. 19).

translationally invariant nonlinear σ model.¹⁹ Such a model would predict $\kappa(T)$ to evolve with doping as shown in Fig. 9. At sufficiently high temperatures the spin system is predicted to be in a “quantum critical” state whose signature is a linear temperature dependence of the inverse correlation length κ . At lower temperatures a crossover to exponential behavior is predicted in the renormalized classical regime ($g < g_c$), while in the quantum disordered regime ($g > g_c$) κ becomes temperature independent at low temperatures. For $g = g_c$, the critical coupling constant for which Néel order disappears even at $T = 0$, this model predicts $\kappa(T) \sim T$ for all temperatures. While it might at first seem possible to interpret the data of Fig. 8(b) using this model, our measurements on more heavily doped samples, which we describe in the next section, deviate significantly from the predictions of the QNL σ M. Instead we have found a very simple empirical relation that yields a very good description for the correlation length of both the data of Fig. 8(b) for Néel ordered samples and data of more heavily doped samples that do not exhibit Néel order.

VII. THE CORRELATION LENGTH IN THE DISORDERED STATE

Using the same technique we applied to undoped La_2CuO_4 , we measured the temperature dependence of the correlation length of four more samples: (1) $\text{La}_{1.98}\text{Sr}_{0.02}\text{CuO}_4$, (2) oxygenated $\text{La}_{1.985}\text{Sr}_{0.015}\text{CuO}_4$, (3) $\text{La}_{1.97}\text{Sr}_{0.03}\text{CuO}_4$, and (4) $\text{La}_{1.96}\text{Sr}_{0.04}\text{CuO}_4$. As grown, sample 2 ordered magnetically at $\sim 80 \text{ K}$. By annealing this sample under oxygen flow ($\sim 800^\circ\text{C}$ for 24 h) we increased its hole concentration such that its low-temperature correlation length approximately equaled that of sample 1. All other samples were used as grown. While we do not know their precise oxygen concentration, the holes donated by oxygen impurities in these samples are only a minor fraction of the total hole content, so that the Sr concentration is a good measure of the

hole concentration in the CuO_2 sheets. Sample 1 showed a crossover to Ising behavior and some 3D diffuse scattering at low temperatures, while in sample 2 no obvious deviation from isotropic 2D behavior was detected. This shows that, as expected, a delicate interplay between thermal effects, doping effects, and the effects of the inter-layer coupling and the exchange anisotropies takes place at the point at which long-range antiferromagnetism disappears. Because of the absence of these complications in sample 2, we chose to study it in detail. Its hole concentration is very close to 2%, and for simplicity we refer to this sample as $\text{La}_{1.98}\text{Sr}_{0.02}\text{CuO}_4$. Results of these experiments have been discussed briefly in Ref. 11.

Figure 10 shows the temperature dependence of the inverse correlation length of the 2, 3, and 4 % hole-doped samples, together with the data for the pure sample. The solid lines are calculated from the simple formula

$$\kappa(x, T) = \kappa(x, 0) + \kappa(0, T). \quad (13)$$

The temperature-dependent inverse length $\kappa(x, 0)$ corresponds to correlation lengths of 150, 65, and 42 Å for the doped samples. $\kappa(0, T)$ is the formula of Hasenfratz and Niedermayer²² [Eq. (8)] with the fitted value of $2\pi\rho_s = 150$ meV. Although it is certainly not unique, this simple formula provides a surprisingly good parametrization of our data for all four samples. The success of this analysis has also led us to reanalyze the data of Fig. 8(b) for samples which exhibit 3D long-range order. The results of fits to Eq. (13), corresponding to $\xi(x, 0)$ of 275 and 140 Å for the $T_N = 190$ - and 90-K samples, respectively, are shown in Fig. 8(b). [The value $\kappa(x, 0)^{-1} = 140$ Å for the $T_N \sim 90$ -K sample is quite uncertain given the evident inhomogeneity of this crystal.] Again, Eq. (13) provides a good description of the data for relatively high temperatures ($T \geq 300$ K) which presumably corresponds to the doped 2D Heisenberg regime. For lower tempera-

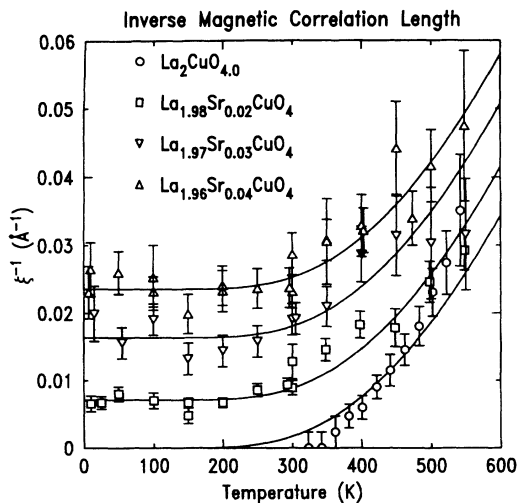


FIG. 10. Inverse magnetic correlation length of four $\text{La}_{2-x}\text{Sr}_x\text{CuO}_4$ samples. The solid lines are calculated from $\kappa(x, T) = \kappa(x, 0) + \kappa(0, T)$. $\text{La}_{1.98}\text{Sr}_{0.02}\text{CuO}_4$ is sample no. 2 in the text.

tures, as $\xi^{-2}(0, T) \sim \xi^{-2}(x, 0) \sim \alpha_{\text{eff}}$, the effects of doping, thermal fluctuations of the Heisenberg model, and the perturbative terms are superposed, and more complicated behavior ensues including, finally, a transition to 3D long-range order. Except for this narrow range in x and T , the temperature and doping dependence of the correlation length for $0 \leq x \leq 0.04$ and $10 \leq T \leq 550$ K follows the simple form (13). We will discuss the implications of this surprising experimental result below.

The temperature dependence of the 2D integrated intensity measured in the $\text{La}_{1.96}\text{Sr}_{0.04}\text{CuO}_4$ sample is shown in Fig. 11. The fact that the intensity decreases gradually with increasing temperature probably means that, due to the cutoff in the energy integration, some part of the relevant magnetic spectrum ($\sim 30\%$ at the highest temperature) is excluded as the temperature is raised. Quite consistent with this observation, we will show below that the characteristic frequency of the spin system is $\omega_0 \sim T/2$. At 500 K this gives $\omega_0 = 21.5$ meV, still significantly below the cutoff energy of 30.5 meV, so that most of the important fluctuations are included in the integration. Once a full theory for $S(\mathbf{Q}, \omega)$ of this spin system becomes available, one may again correct the data for the effects of the cutoff. However, the above arguments show that any such correction is unlikely to be significant.

Equation (13) has a broad range of implications for the theory of doped copper oxides. First, it is manifestly inconsistent with a number of theoretical predictions for the magnetic state of these materials: A Curie-Weiss law, $\xi \sim (T - T_0)^{-1/2}$, which has been proposed by several authors^{36,37} clearly does not describe our data. For $g > g_c$ the QNL σ M with a doping-dependent effective coupling constant does predict a correlation length of the form of Eq. (13).^{19,35} In this description the analogue of $\kappa(0, T)$ has the linear temperature-dependence characteristic of the quantum critical regime for temperatures higher than an undetermined crossover temperature. By fitting the zero-temperature correlation length and the crossover temperature for each data set, the data for the 3 and 4 % hole-doped samples can certainly be reconciled with this scenario. We note, however, that the crossover tempera-

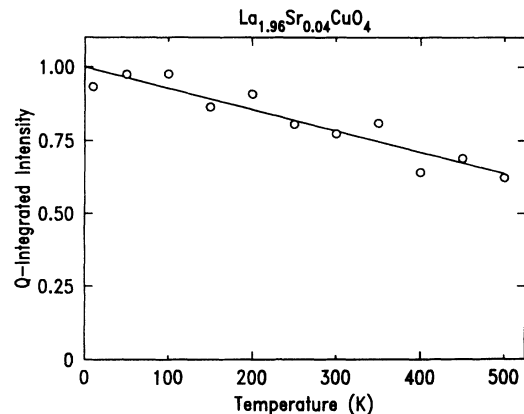


FIG. 11. Q integrated intensities of the energy-integrating scans taken on the $\text{La}_{1.96}\text{Sr}_{0.04}\text{CuO}_4$ sample.

ture emerges naturally in the one-parameter fit to the empirical equation (13) discussed above. More seriously, according to the prediction of Fig. 9, $\kappa(T)$ should be linear over a wide range of temperatures for the 2% hole-doped sample. Instead, we find that $\kappa(T)$ is approximately temperature independent below room temperature and then increases like $\kappa(0, T)$ for $T > 300$ K.

At high dopant concentrations, the correlation length is of the order of the average separation between the holes, i.e., $\xi(x, 0) \sim a/\sqrt{x}$.³⁸ While the correlation lengths measured in our samples are systematically longer than this simple relation would predict, they are of the same order of magnitude and approach this limit for increasing x . At least for the 2% hole-doped sample, the perturbative terms still enhance the low-temperature correlation length. We are not aware of any quantitative predictions for the correlation length in doped antiferromagnets that take into account both thermal and doping effects. However, in the zero-temperature limit a number of numerical simulations have been reported. The numerical implementation of a simple model first proposed phenomenologically by Aharony *et al.*⁹ yields quantitative results: Based on the approximation that the holes are localized on the oxygen atoms in the CuO_2 planes and thus lead to the formation of magnetic polarons with associated long-range distortions of the antiferromagnetic background, Gooding and Mailhot³⁹ obtained $\xi(x=0.03, 0) = (55.8 \pm 12)$ Å and $\xi(x=0.04, 0) = (33.2 \pm 2.4)$ Å. The close agreement with the values deduced from our measurements suggests that a model of this type may indeed be an adequate description of the zero-temperature static correlation function. As we noted above, our experimental data do not allow a more elaborate line-shape analysis, so that we cannot explore this issue in more detail at present.

A priori, there exist two possible scenarios for the multicritical behavior near $x = T = 0$ in two dimensions. In the first, $x = 0$ is an unstable fixed point, so that the correlation length $\xi(x, 0)$ decreases monotonically with increasing x . In this case, we expect the scaling form

$$\kappa(x, T) = \kappa(x, 0) f[\kappa(0, T)/\kappa(x, 0)],$$

with the scaling function $f(y)$ approaching the behavior $f(y) \sim y$ for $y \gg 1$. For small y , it is reasonable to expect a linear behavior, $f(y) = 1 + ay + O(y^2)$. Neglecting the higher-order terms, the truncated expansion $f(y) = 1 + y$ reproduces both the small- and the large- y limits and yields Eq. (13).

In the second scenario, there may exist an unstable fixed point at some finite $x_c > 0$, while the point $x = 0$ is stable. This scenario would maintain long-range order for $0 < x < x_c$ and $T = 0$. At $T > 0$ and $x \sim x_c$ one would then expect that $\kappa(x_c, T)$ be governed by the scaling properties near x_c , and the temperature dependence of $\kappa(x_c, T)$ may be very different from that of $\kappa(0, T)$. Birgeneau *et al.*⁴⁰ have shown experimentally that this scenario applies to diluted magnets close to their percolation thresholds. In the $\text{La}_{2-x}\text{Sr}_x\text{CuO}_4$ case, the fact that we observe consistency with Eq. (13) over a range of $x > 0$ seems to support the first model in which the Néel

state of the underlying 2D isotropic spin system becomes unstable towards the formation of a phase with finite correlation length even for an infinitesimally small concentration of holes. Three-dimensional order is nevertheless achieved up to dopant concentrations such that $\alpha_{\text{eff}}^2(x, 0) \sim 1$.

At the critical dopant concentration a delicate balance exists between the effects of the interlayer coupling, which drives the spin system towards long-range order, and the effects of doping, which counteracts this tendency. As a manifestation of this delicacy, we have seen that three different samples with $\xi(x, 0) \approx 150$ Å exhibit very different low-temperature behavior: Oxygenated La_2CuO_4 [Fig. 8(b)] orders at $T_N \approx 90$ K, as-grown $\text{La}_{1.98}\text{Sr}_{0.02}\text{CuO}_4$ exhibits a crossover to Ising behavior at low T with attendant 3D diffuse scattering, and the instantaneous correlation function of oxygenated $\text{La}_{1.985}\text{Sr}_{0.015}\text{CuO}_4$ is T independent below room temperature (Fig. 10). We cannot, at present, definitely decide whether $T = 0$ Néel order for the underlying 2D Heisenberg model disappears at $x = 0$ or whether it persists to a small but finite hole concentration. However, as argued above, the fact that Eq. (13) works even for an extremely small hole concentration strongly suggests that $x = 0$ is indeed the multicritical concentration for the idealized 2D Heisenberg system.

In conclusion, we have found that in this crossover regime the correlation length at low temperatures is temperature independent and dominated by the holes. At higher temperatures, however, as shorter and shorter length scales are probed, the correlation length progressively approaches that of the pure system. The exponential divergence of the correlation length of undoped La_2CuO_4 is still clearly recognizable in $\text{La}_{1.96}\text{Sr}_{0.04}\text{CuO}_4$, with a zone-boundary energy scale that is not much reduced. Consequently, we expect the magnetic dynamics at high energies to be quite similar to the undoped quantum antiferromagnet, while the interaction between the carriers and the antiferromagnetically correlated spin system may lead to different behavior at low energies. As we will see now, the low-energy spin dynamics in the doped compounds is indeed quite novel.

VIII. SPIN DYNAMICS IN $\text{La}_{1.96}\text{Sr}_{0.04}\text{CuO}_4$

A. Intermediate energy excitations

We have performed an extensive set of inelastic-scattering measurements for the sample of composition $\text{La}_{1.96}\text{Sr}_{0.04}\text{CuO}_4$ with a low-temperature correlation length of 42 Å. The measurements span the energy range $0.75 \leq \omega \leq 45$ meV for temperatures $1.5 \leq T \leq 500$ K.

Since many theories predict low-energy spin excitations to occur not only at the (100) position [or (π, π) in square lattice notation], but also at other high-symmetry positions, we first oriented our sample such that the entire in-plane reciprocal space was accessible. The data were taken at the BT9 spectrometer at NIST. The incident neutron energy was held fixed at 30.5 meV, and the collimator configuration was 40'-40'-S-40'-80'. The

(200) reflection of pyrolytic graphite was used as both monochromator and analyzer, and a pyrolytic graphite filter was inserted into the incoming beam to minimize contamination from higher harmonics. Figure 12 shows scans at $\omega=6$ meV and temperatures 10 and 300 K at the $(\frac{1}{2}0\frac{1}{2})$ position [corresponding to $(\pi,0)$ in square lattice notation] and, for comparison, at the (100) position. Clearly, no scattering above background is observed in the vicinity of $(\frac{1}{2}0\frac{1}{2})$. We also performed similar scans at (110), with identical results. This rules out models like the “flux phase”⁴¹ or frustrated Heisenberg models⁴² as a description of our data.

As mentioned in Sec. IV, the range of energy transfers for this particular sample orientation is restricted to $4.5 \leq \omega \leq 12$ meV. In Fig. 13, we present a series of longitudinal and transverse scans through the (100) position [scans *A* and *B* in Fig. 2(b)] at $\omega=4.5, 6, 9,$ and 12 meV taken in this configuration. These data are of excellent quality: Up to the highest temperatures the background remained flat and featureless, and good signal-to-noise ratios could be achieved throughout the entire temperature range. The data quality is high because the correlation length is still quite long in this sample: For a correlation length of 20 Å as found for superconducting compositions the peak intensity would be reduced by a factor of roughly 4, and the experiment would have been much more difficult.

In contrast to the spin correlations in superconducting $\text{La}_{2-x}\text{Sr}_x\text{CuO}_4$ samples, all measured peaks are commensurate within the resolution of the experiment. The apparent anisotropy of the peak shape is entirely due to an anisotropy of the experimental resolution function. The solid lines in Fig. 13 are, in fact, fits of isotropic 2D

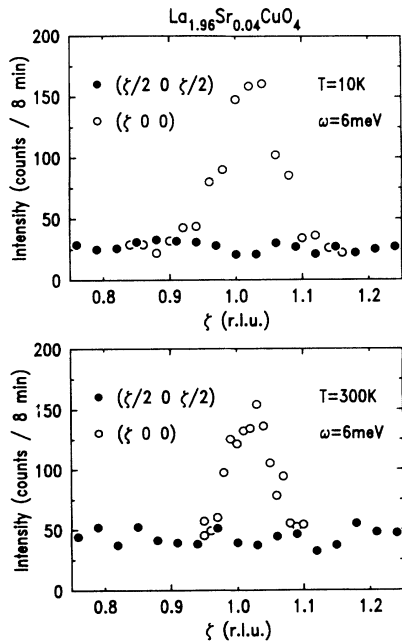


FIG. 12. Scattering intensity at $\omega=6$ meV near the positions (100), i.e., $(\pi\pi)$ in square lattice notation, and $(\frac{1}{2}0\frac{1}{2})$, i.e., $(\pi,0)$ in square lattice notation, for $\text{La}_{1.96}\text{Sr}_{0.04}\text{CuO}_4$.

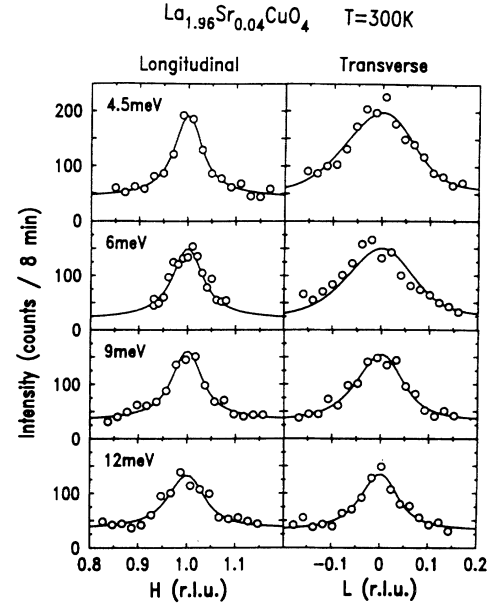


FIG. 13. Room-temperature inelastic-scattering intensity at $Q=(100)$ for four different energies in $\text{La}_{1.96}\text{Sr}_{0.04}\text{CuO}_4$. The solid lines are the results of fits to isotropic 2D Lorentzians of width $\kappa=0.02$ r.l.u., convoluted with the experimental resolution function.

Lorentzians, convoluted with the resolution function. The width was held fixed at $\kappa=0.02$ r.l.u., as measured from the instantaneous correlation function above, and only the amplitude was adjusted. This simple procedure provided an adequate description of all data taken in this configuration.

We first extended the dynamic range of our experiment to encompass fluctuations down to $\omega=2$ meV and up to $\omega=45$ meV. As discussed in Sec. IV of this work, this required a reorientation of the 2D excitation rod into the scattering plane. These experiments were carried out at the H7 spectrometer at Brookhaven with a collimator configuration $40'-40'-40'-80'$. Again, a pyrolytic graphite filter was inserted into the beam path. For the $\omega=2-$ and $3-$ meV data, the incident neutron energy was held fixed at 14.7 meV, and the scans were taken through the $(1,-0.3,0)$ position [scan *C* in Fig. 2(c)]. Some of these data are presented in Fig. 14. For the data above $\omega=12$ meV, the final neutron energy was held at 30.5 meV, and various positions along the 2D rod were selected in order to maximize the scattering intensity. A representative scan for $\omega=35$ meV at room temperature is shown in Fig. 15. We also chose several overlap points to match the three data sets.

From the measurements above we found that the scattering was isotropic around the (100) position. We therefore again performed fits to isotropic 2D Lorentzians in order to extract the intrinsic scattering intensity. For excitation energies below 20 meV, Lorentzians of fixed width 0.02 r.l.u. again yielded an adequate description of our data. A larger linewidth was necessary to fit the data for $\omega \geq 20$ meV, as demonstrated for $\omega=35$ meV

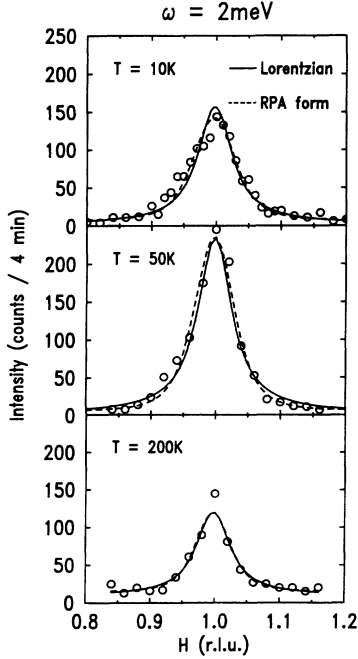


FIG. 14. Scans along $(H, -0.3, 0)$ at $\omega = 2$ meV for $\text{La}_{1.96}\text{Sr}_{0.04}\text{CuO}_4$. The solid lines are the results of fits to isotropic 2D Lorentzians of intrinsic width $\kappa = 0.02$ r.l.u., convoluted with the experimental resolution function. The dashed line is the prediction of the random-phase approximation (RPA) Lorentzian squared form, Eq. (16).

in Fig. 15. A summary of the fitted widths is provided in the inset in Fig. 16. The increasing linewidth as a function of ω reflects a crossover to propagating spin waves, as expected for $\omega \geq c\kappa \approx 20$ meV. This effect, which has been mapped out in more detail by Hayden *et al.*⁴³ for $\text{La}_{1.95}\text{Ba}_{0.05}\text{CuO}_4$, underscores our point above: The spin

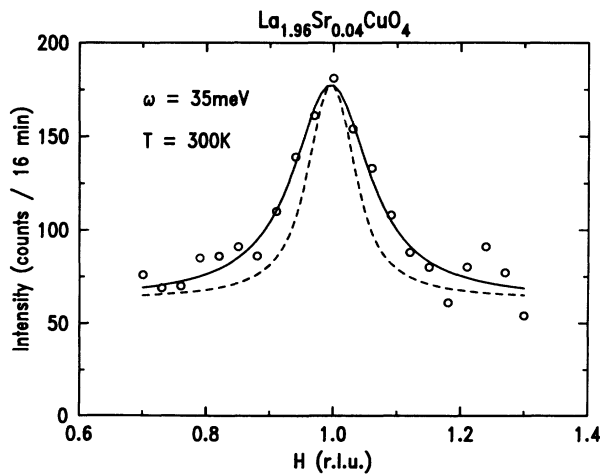


FIG. 15. Scan along $(H, -3.5, 0)$ at $\omega = 35$ meV. The solid line is the result of a fit to a 2D Lorentzian of width 0.05 r.l.u., convoluted with the resolution function. The dashed line results if the width is kept fixed at 0.02 r.l.u., as in Figs. 13 and 14.

dynamics at short length scales, corresponding to high excitation energies, are not qualitatively altered from those of the pure system.

Since the low-energy measurements are close to resolution limited, the \mathbf{Q} integrated intensity, that is, the quantity $\int d^2\mathbf{Q}S(\mathbf{Q}, \omega)$, can be extracted from our data most reliably. Figure 17 presents a synopsis of the resolution-corrected 2D integrated intensities obtained in this manner. At 10 K the intensity is a decreasing function of ω for low energies and approaches a constant for higher energies. This is shown more clearly in Fig. 16. A small correction for the magnetic form factor was applied to the data for $\omega \geq 20$ meV. As a function of temperature, the intensity at each energy rises and peaks at a temperature $T \approx 2\omega$. This led us to divide out the zero-temperature response and plot the temperature-dependent part as a function of ω/T .

The result is shown in Fig. 18. For this figure we have converted our data to the \mathbf{Q} integrated dynamical susceptibility using Eq. (4), and we have chosen the overall scale such that $\int d^2\mathbf{Q}\chi''(\mathbf{Q}, \omega) \rightarrow 1$ for large ω . The result shown in Fig. 18 is remarkable: Plotted in this scaled fashion, our entire data set for $2 \leq \omega \leq 45$ meV and $10 \leq T \leq 500$ K collapses onto a single curve. These data cover a range in ω/T of nearly three decades. As we will see below, the discovery of this simple form for $\chi''(\mathbf{Q}, \omega)$ allows us to relate the microscopic magnetic properties measured in our experiment with other physical properties of these materials.

In order to obtain a parametrization of the measured $\chi''(\mathbf{Q}, \omega)$, we have used the heuristic form

$$\int d^2\mathbf{Q}\chi''(\mathbf{Q}, \omega) = I(|\omega|, 0) \arctan \left[a_1 \frac{\omega}{T} + a_3 \left(\frac{\omega}{T} \right)^3 \right]. \quad (14)$$

$I(|\omega|, 0)$ is the zero-temperature response shown in Fig.

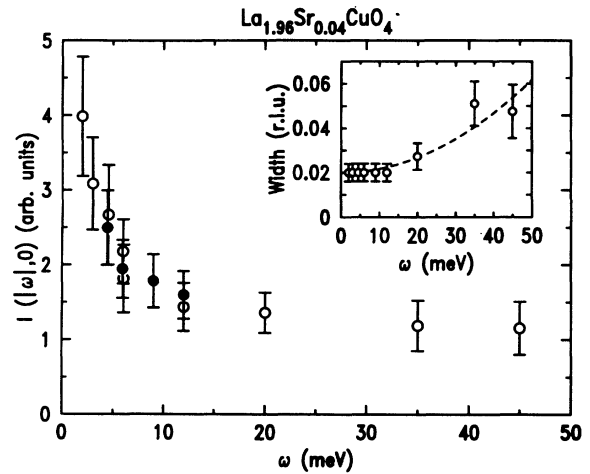


FIG. 16. Energy dependence of the \mathbf{Q} integrated intensity at $T = 10$ K. For the energies shown here the intensity is temperature independent below this temperature, and the plot therefore represents the zero-temperature response $I(|\omega|, 0)$. The inset shows the intrinsic width of the scattering profiles.

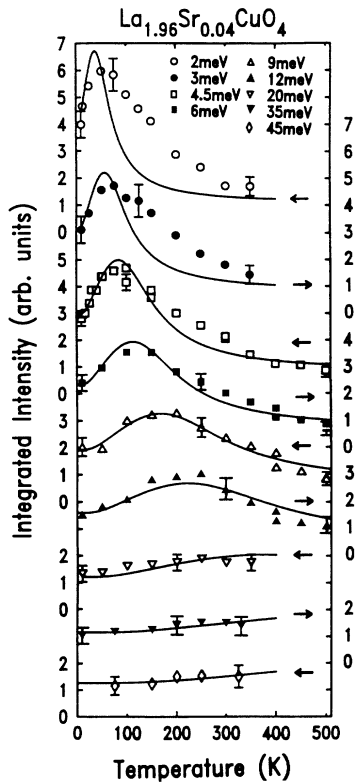


FIG. 17. Scattering intensity integrated around the $(\pi\pi)$ position in reciprocal space for $2 \leq \omega \leq 45$ meV. The solid lines represent a heuristic parametrization of this data set that is homogeneous in ω/T , as discussed in the text.

16. As required by time-reversal symmetry, this function is odd in ω . The best fit of this form to our data with $a_1 = 0.43$ and $a_3 = 10.5$ is represented as the solid line in Fig. 18. The solid curves in Fig. 17 are also calculated from this expression. Equation (14) obviously gives a very good description of our data, except for some sys-

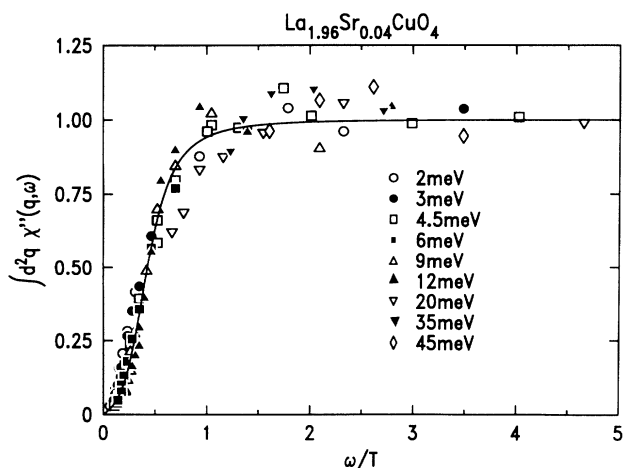


FIG. 18. Normalized integrated spin susceptibility as a function of the scaling variable ω/T . The solid line is the function $2/\pi \tan^{-1}[a_1 \omega/T + a_3 (\omega/T)^3]$ with $a_1 = 0.43$ and 10.5 .

tematic deviations for the lowest energies $\omega = 2$ and 3 meV.

The simplest functional form for the nonintegrated $\chi''(\mathbf{Q}, \omega)$ consistent with all of our data is therefore simply the product of the right-hand side of Eq. (14) with the Lorentzian static structure factor determined in the energy-integrating experiments above. However, a simple product of q -dependent and ω -dependent terms is inconsistent with the different temperature dependence of copper and oxygen relaxation rates measured in NMR experiments.⁴⁴ We discuss a more physically meaningful functional form of $\chi(\mathbf{Q}, \omega)$ in Sec. IX.

An ω/T scaling relation for the dynamical susceptibility of $\text{La}_{1.95}\text{Ba}_{0.05}\text{CuO}_4$ was first reported by Hayden *et al.*⁴³ for a limited range of temperatures $80 \leq T \leq 260$ K. The simple function $\int d^2Q \chi''(\mathbf{Q}, \omega) \sim \arctan(\alpha\omega/T)$ proved to be consistent with these early measurements. The considerably more accurate and extensive measurements reported here require the more elaborate form Eq. (14). Although the difference between the two expressions is small for temperatures near room temperature, our determination of the correct form is actually quite important, since a data analysis based on an overly simplified functional form can give rise to misleading conclusions: Specifically, Hayden *et al.*⁴³ report a drastic change in the low-energy spin dynamics at 80 K, where the logarithmic conduction effects become relevant. By contrast, Eq. (14) describes our data equally well above and below 80 K. Thus, the spin dynamics are apparently unaffected by the crossover to logarithmic resistive behavior below 80 K. This is hardly surprising considering the fact that we have estimated the localization length to be substantially larger than the magnetic correlation length in this sample (Sec. III).

B. Low-energy excitations and central peak

Sternlieb *et al.*¹⁰ have reported the appearance of frozen moments at temperatures below 6 K in a nonsuperconducting sample of $\text{La}_{1.94}\text{Sr}_{0.06}\text{CuO}_4$. At somewhat higher temperatures they detected an anomalous increase in the quasielastic neutron-scattering intensity. These observations were interpreted in analogy to conventional spin glasses. In order to explore a possible relation of this effect with the charge carrier localization behavior observed at low temperatures in our sample, we have measured the temperature dependence of the magnetic excitations at $\omega = 0.75$ meV, $\omega = 1$ meV, and around the elastic position $\omega = 0$.

This experiment was again performed at the H7 spectrometer at Brookhaven. In order to collect meaningful data at these low energies, we had to tighten the energy resolution of our spectrometer, and we initially chose the collimator configuration 20'-40'-S-20'-80' with an incident neutron energy of 14.7 meV. A resolution calculation yields an energy resolution of ~ 0.9 -meV FWHM under these conditions. We took several scans through the $(1, -0.3, 0)$ point on the 2D excitation rod for $1.5 \leq T \leq 72$ K. These scans were again characterized by a temperature-independent intrinsic width equal to the magnetic correlation length, so that the \mathbf{Q} integrated in-

tensity was directly proportional to the peak intensity at $Q=(\pi, \pi)$. Most of the results shown in Fig. 19(a) are therefore simply background-corrected peak intensities. Both the $\omega=0.75$ - and the $\omega=1$ -meV intensities peak at a temperature $T=2\omega$, demonstrating that the scaling description developed in the previous section is not fundamentally altered at this low-energy scale. Since the full width of the experimental resolution function centered at $\omega=0.75$ meV encompasses the $\omega=0$ position and the measured intensity at this energy therefore contains a significant contribution of the central peak as we will discuss below, it is difficult to draw quantitative conclusions from the $\omega=0.75$ -meV data. The data at $\omega=1$ meV, on the other hand, are unaffected by $\omega=0$ contamination. While the temperature dependence of the 1-meV intensity looks qualitatively similar to the 2-meV intensity shown in Fig. 16, a close examination reveals a significant deviation from the scaling function at low temperatures: In accordance with the trend shown in Fig. 16, the peak intensity is larger at 1 meV than at 2 meV, but at $T=1.5$ K the two intensities are approximately equal.

This is demonstrated more clearly in Fig. 20, where we have normalized the 1-meV data to the scaling curve of Fig. 18 at the peak intensity ($T=23$ K). About one-half of the 1-meV intensity is lost at the lowest temperatures.

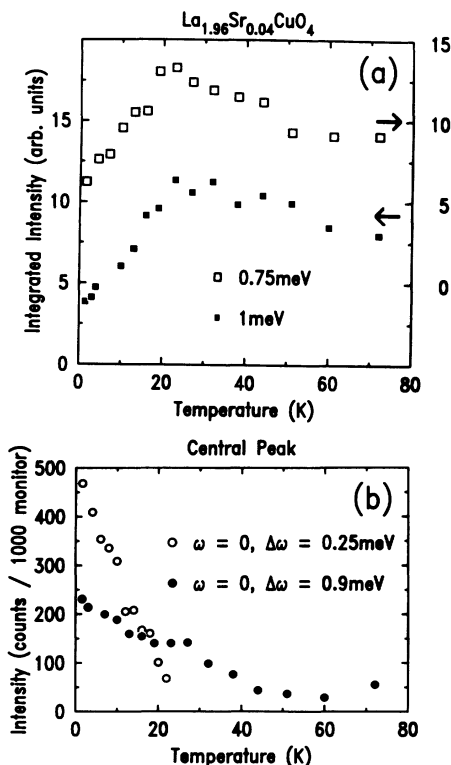


FIG. 19. (a) Q integrated intensity for $\omega=0.75$ and 1 meV. (b) Scattering intensity in two windows around the elastic position. The window $\Delta\omega=0.25$ -meV FWHM corresponds to the spectrometer configuration, $E_i=5$ meV, $40^\circ\text{-}40^\circ\text{-}S\text{-}40^\circ\text{-}80^\circ$. The window $\Delta\omega=0.9$ -meV FWHM corresponds to $E_i=14.7$ meV, $20^\circ\text{-}40^\circ\text{-}S\text{-}20^\circ\text{-}80^\circ$. The data taken in the two configurations are not normalized with respect to one another.

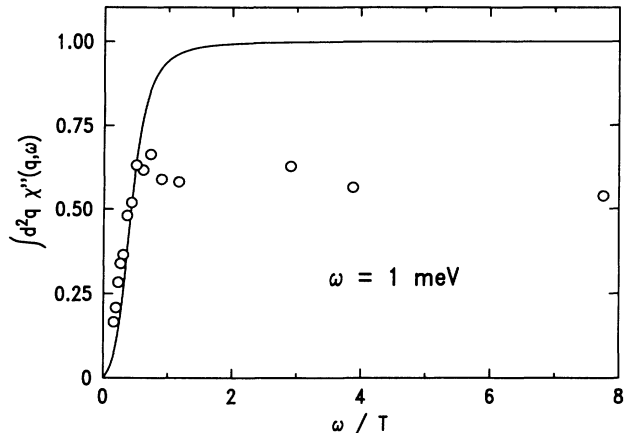


FIG. 20. Integrated spin susceptibility for $\omega=1$ meV, normalized at $T=23$ K to the scaling curve of Fig. 18.

The most likely explanation of this is a residual effect of the spin-XY anisotropy, which creates an effective gap for out-of-plane spin fluctuations at low temperatures. An evaluation of the geometrical factors of Eq. (2) shows that at elevated temperatures, where the spin system is isotropic, the signal in the vicinity of the (100) position is comprised of equal contributions of in-plane and out-of-plane spin fluctuations. In principle, in-plane and out-of-plane correlation functions can be separated experimentally by systematically varying the momentum transfer coordinate K . A detailed study of this kind is planned for the future. Our tentative conclusion that at low temperatures and energies below 2 meV only in-plane spin fluctuations can be excited means that under these conditions the system effectively behaves like a 2D XY system. If this interpretation is correct, the anisotropy gap is actually surprisingly close to its value in lightly doped La_2CuO_4 (~ 2.5 meV).²⁸ Because of the absence of long-range order there is apparently no analogue of the antisymmetric exchange gap for the in-plane excitations of the pure system.

At the nominal $\omega=0$ position in this spectrometer configuration, one measures a weighted superposition of excitations in an energy window of ± 0.5 meV centered around $\omega=0$. As shown in Fig. 19(b), the measured intensity gradually decreases as the temperature is raised from $T=1.5$ K and reaches a small saturation value at $T\sim 40$ K. This is qualitatively consistent with an extrapolation of the scaling function Eq. (14) to energies below 1 meV: As the temperature is raised, the characteristic energy $\omega=T/2$ gradually moves out of the energy window given by the experimental resolution, so that the measured intensity is reduced.

In order to reach even smaller excitation energies, we further tightened the energy resolution of our spectrometer by changing the incident neutron energy to 5 meV with a collimator configuration of $40^\circ\text{-}40^\circ\text{-}S\text{-}80^\circ\text{-}80^\circ$. A beryllium filter was used before the sample to eliminate contamination of the incident beam by higher harmonics. Under these conditions the energy resolution becomes ~ 0.25 -meV FWHM. The temperature dependence of

the excitations integrated over this energy window is also shown in Fig. 19(b). While this may at first seem consistent with the gradual slowing of the spin fluctuations discussed above, we will see now that the excitations measured in this experimental configuration are distinctly different from the inelastic spectrum we have mapped out so far.

Figure 21 dramatically illustrates this fact: Even at $T = 6$ K, where the 0.5-meV intensity should be near its maximum according to our analysis above, the intensity at the elastic position is at least 1 order of magnitude greater than the $\omega = 0.5$ -meV intensity. Indeed, due to the substantially reduced resolution volume we could not observe any scattering intensity at $\omega = 0.5$ meV within a reasonable counting time. This, in turn, means that the part of the spectrum that gives rise to the quasielastic peak must be sharply concentrated around $\omega = 0$. Consistent with this observation, we found that the quasielastic peak was perfectly resolution limited, so that its intrinsic energy scale was much less than 0.1 meV.

Figure 21 also shows that the intrinsic width in momentum of the central peak is again equal to the inverse magnetic correlation length. Since the spatial range of the magnetic correlations is limited by the charge carriers, it is reasonable to associate the central peak with a random static spin distortion created by the holes,^{9,38} which are already well localized at these temperatures. Central peaks are observed in many systems in which impurities create random fields.⁴⁵ An interesting variation of this phenomenon is the 2D XY magnets, where thermally excited vortices give rise to central peaks of very low intrinsic energy scales.^{46,47} Since spin systems of XY symmetry are more susceptible to topological excitation than isotropic spin systems, it may not be accidental that the appearance of the central peak coincides with the opening of the XY gap around ~ 20 K. The generic functional form for central peaks is a squared Lorentzian in momentum.^{45,47} Unfortunately, a very large signal-to-background ratio is required to distinguish unequivocally between Lorentzian and squared Lorentzian line shapes.

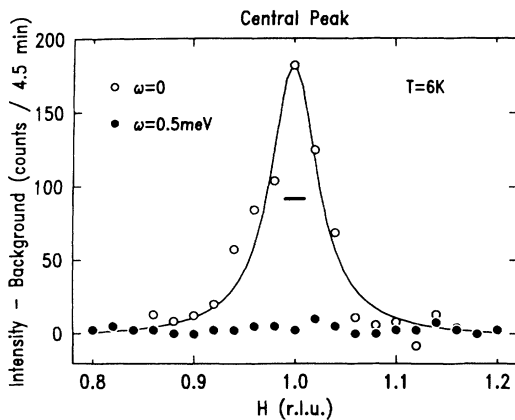


FIG. 21. Scans along $(H, -0.3, 0)$ at the elastic position and at $\omega = 0.5$ meV. The line is the result of a fit to a 2D Lorentzian of fixed width $\kappa = 0.02$ r.l.u., convoluted with the experimental resolution function whose FWHM is represented by the bar.

This requirement is not met by any of the data we have thus far been able to take on our sample. More work on different samples is therefore necessary to clarify the connection between the central peak, the anisotropy gap, and the localization of the charge carriers.

IX. DISCUSSION

In Sec. VIII A we have found that Eq. (14), together with a Lorentzian static structure factor, is an adequate description for the dynamical susceptibility measured in our experiment. In order to arrive at a physical understanding of this behavior, we now discuss the dynamical susceptibility from a more general perspective. Several groups^{36,37,48,49} have used the random-phase approximation to calculate the effect of electronic correlations on the susceptibility $\chi_0(\mathbf{Q}, \omega)$ of an underlying noninteracting spin system. One generally writes

$$\chi(\mathbf{Q}, \omega) = \frac{\chi_0(\mathbf{Q}, \omega)}{1 - J(\mathbf{Q})\chi_0(\mathbf{Q}, \omega)}. \quad (15)$$

We have found experimentally that the interaction term $J(\mathbf{Q})$ remains peaked around the (π, π) position. We can therefore expand $J(\mathbf{Q})$ in terms of $\mathbf{q} = \mathbf{Q} - (\pi, \pi)$ and find for small \mathbf{q} and ω

$$\chi''(\mathbf{Q}, \omega) = \frac{\chi_0''(q, \omega)}{(1 + q^2\xi^2)^2 + [\chi_0''(q, \omega)]^2}. \quad (16)$$

In disordered antiferromagnets one generally finds relaxational behavior, $\chi_0''(q, \omega) = \omega/\Gamma$, where Γ is the relaxation rate. In mean-field theory, the magnetic correlations reduce the relaxation rate such that $\Gamma = \Gamma_0\xi^{-2}$. Several authors^{36,37} have used this simple model in the context of the copper oxides. In conjunction with a hypothesized Curie-Weiss law, $\xi \sim T^{-1/2}$, the \mathbf{Q} integrated susceptibility in this model is homogeneous in ω/T . Below we will find this observation useful for comparison with the results of our studies. From the measurements shown in Fig. 10 we know that the ω/T scaling of $\chi''(\mathbf{Q}, \omega)$ occurs in spite of the fact that $\xi \sim \text{const}$ over most of the temperature range, and that the spin dynamics is therefore very different from that of a conventional disordered antiferromagnet. If one nevertheless writes ad hoc $\Gamma \sim T$ and adds a cubic term in ω/T , one arrives at Eq. (14). While Eq. (14) is obviously a very good description for the \mathbf{Q} integrated response, this modified form of the mean-field expression for $\chi(\mathbf{Q}, \omega)$ would predict a divergence of the peak width as a function of momentum at fixed energy at low temperatures, whereas the width of the observed peaks is temperature independent.

This problem is alleviated if we set

$$\chi_0''(q, \omega) = A \tanh[a_1(\omega/T) + a_3(\omega/T)^3].$$

This substitution is motivated by the work of Virosztek and Ruvalds,⁵⁰ who show that a dynamical susceptibility homogeneous in ω/T can arise from nesting effects in a Fermi liquid. In the vicinity of the (π, π) position, these authors obtain $\chi_0'' = \tanh(\gamma\omega/T)$. With the above replacement, Eq. (16) then predicts a roughly temperature-independent width of the inelastic-scattering profiles,

consistent with the experimental observation. The predicted shape of both inelastic and energy-integrated profiles is close to a squared Lorentzian in q . We have noted above that our present data do not allow us to differentiate between Lorentzian and squared Lorentzian line shapes. This is shown explicitly in Fig. 14, where we display the result of fits to Eq. (16) with

$$\chi''_0(q, \omega) = A \tanh[a_1(\omega/T) + a_3(\omega/T)^3]$$

as well as fits to simple Lorentzians. Both functional forms obviously yield equally good descriptions of our data. Integrated over Q , we obtain

$$\int d^2Q \chi''(Q, \omega) = \arctan\{\tanh[a_1(\omega/T) + a_3(\omega/T)^3]\},$$

a form whose characteristics are very similar to Eq. (14) and therefore definitely consistent with our data. In conclusion, Eq. (15) with an expression for $\chi''_0(Q, \omega)$ reminiscent of a nested Fermi liquid is the simplest functional form for the dynamical susceptibility known to us that is both physically meaningful and consistent with all of our data.

Equations (14) and (16) are also consistent with the ‘‘marginal Fermi liquid’’ model of Varma *et al.*⁵¹ which is based on the hypothesis $\chi''(Q, \omega) = \omega/T$ for $\omega/T \ll 1$, and $= 1$ for $\omega/T \gg 1$. ω/T scaling effects over a limited range of ω and T also arise in the Fermi-liquid model of Levin and co-workers.⁴⁹ Our samples are relatively lightly doped and retain many features of the local moment system at zero doping, such as the anisotropy gap at low temperatures and the high-temperature magnetic correlation length. Any model based on itinerant Cu spins would have to be modified to take these features into account. Theory must also explain the approximate constancy with doping of the magnetic cross section.

Without committing ourselves to any specific microscopic model for the copper oxides, we can also start from the empirical parametrization of the spin fluctuation spectrum determined very accurately in our experiment and derive in a phenomenological manner the consequences of this spectrum for other physical quantities.

There is ample evidence for strong interactions between the fluctuating spin system and the charge carriers; examples include the isotropic negative magnetoresistance and the strongly doping dependent magnetic correlation length. Moriya, Takahashi, and Ueda³⁶ have derived a general formula for the scattering of charged quasiparticles from antiferromagnetic fluctuations:

$$\rho(T) \sim T \int_{-\infty}^{\infty} d\left[\frac{\omega}{T}\right] \frac{\omega}{T} \frac{e^{\omega/T}}{(e^{\omega/T} - 1)^2} \int d^2Q \chi''(Q, \omega) \quad (17)$$

within the context of nearly antiferromagnetic Fermi-liquid theory. We have computed this integral numerically using the expression for $\int d^2Q \chi''(Q, \omega)$, Eq. (14), deduced from our data. For this purpose, we parametrized the zero-temperature response shown in Fig. 16 ad hoc as

$$I(|\omega|, 0) = B + (A - B)/[1 + (\omega/\omega_0)^2],$$

with $A = 4.8$, $B = 1.2$, and $\omega_0 = 3.5$ meV. The result is shown in Fig. 22. The resistivity arising from the experimentally observed spin fluctuation spectrum is linear in temperature above ~ 100 K and thus provides an explanation for the measured resistivity shown in Fig. 4. Inspection of Eq. (17) shows that the linearity in temperature is due to the observed homogeneity of $\int d^2Q \chi''(Q, \omega)$ in ω/T . Deviations from this homogeneity lead to nonlinear behavior of the predicted resistivity below ~ 100 K. However, the derivation of Eq. (17) is based on the Boltzmann equation and is therefore no longer valid below the onset of weak localization effects around this temperature. A more detailed microscopic theoretical treatment is necessary to understand the behavior in this regime, as well as the observed approximate H/T scaling of the magnetoresistance.¹⁴ The significance of the nonvanishing $T=0$ intercept of the T linear part of the resistivity derived from Eq. (17) is also unclear at present.

A resistivity linear in temperature is one of the most striking features of the normal state of the copper-oxide superconductors. Inspired by the promising analysis above, the temperature dependence of the dynamical susceptibility of several other doped cuprates has been measured: Endoh *et al.*⁵² find that Eq. (14) with identical parameters also yields an excellent description of the dynamical susceptibility of a $\text{La}_{1.98}\text{Sr}_{0.02}\text{CuO}_4$ sample with a correlation length of ~ 150 Å, almost a factor of 4 greater than the correlation length of the $\text{La}_{1.96}\text{Sr}_{0.04}\text{CuO}_4$ sample we investigated. Birgeneau *et al.*⁵³ have recently reported ω/T scaling effects in superconducting $\text{YBa}_2\text{Cu}_3\text{O}_{6.5}$ with $\xi \sim 10$ Å. Equation (14) also applies to this compound, but the cubic term vanishes and $I(|\omega|, 0)$ is an initially increasing function of ω . Nevertheless, the resistivity calculated from Eq. (17) and the presently available data for $\chi''(Q, \omega)$ is also linear in

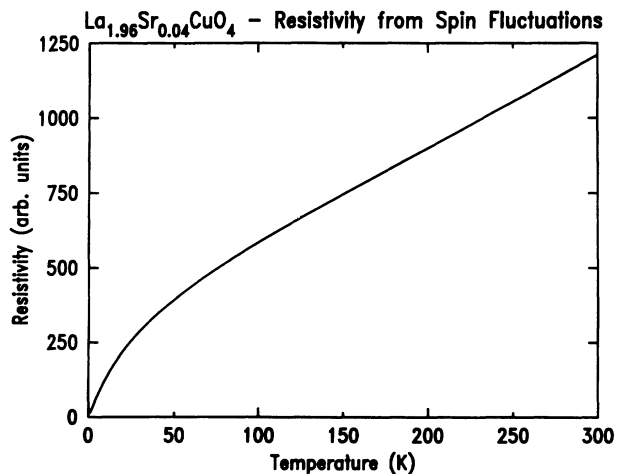


FIG. 22. Resistivity due to scattering of charged quasiparticles from the experimentally determined spin fluctuations spectrum, calculated according to Moriya, Takahashi, and Ueda (Ref. 36).

T for $T \geq 100$ K. Thus, our analysis seems to apply generally to the metallic regime of the doped copper oxides, at least for relatively modest doping.

In the more heavily doped samples the appearance of gaps in the spin fluctuation spectrum at low temperatures and the inherent difficulty of the experiments have thus far prevented a similarly extensive neutron-scattering study. However, NMR experiments, which have been carried out both for lightly doped and for heavily doped materials,⁵⁴ generally seem to require $\lim_{\omega \rightarrow 0} \int d^2Q \chi''(\mathbf{Q}, \omega) \sim \omega/T$, consistent with our Eq. (14).

Recently, Moriya and Takahashi⁵⁵ extended Eq. (17) to describe the optical conductivity and by assuming $\xi \sim T^{-1/2}$ are able to explain the experimental result⁵⁶ $\tau^{-1}(\omega) \sim \max(T, \omega)$, where $\tau^{-1}(\omega)$ is the inelastic-scattering rate. Again, this result rests only on the homogeneity of the \mathbf{Q} integrated susceptibility in ω/T and therefore directly transfers to our analysis. The simple parametrization of the inelastic-scattering rate was found in a very thorough study of the $\text{YBa}_2\text{Cu}_3\text{O}_{6+x}$ system.⁵⁶ The $\text{La}_{2-x}\text{Sr}_x\text{CuO}_4$ system seems to exhibit more complicated behavior,⁵⁷ but the studies undertaken thus far have not been as exhaustive as for $\text{YBa}_2\text{Cu}_3\text{O}_{6+x}$. Not-

withstanding this potential complication, scattering of charged excitations from the spin fluctuation spectrum measured in our experiments seems capable of explaining many of the unusual features of both the dc and the ac conductivities.

Clearly, the theory for the metallic state of the doped copper oxides still requires significant development. We hope that our results will prove useful in constructing a viable microscopic model for the unusual electronic properties of these materials.

ACKNOWLEDGMENTS

The work at MIT was supported by National Science Foundation Grant Nos. DMR 90-22933, DMR 90-14839, and DMR 90-07825. Work at Brookhaven was carried out under Contract No. DE-ACO2-76CH0016, Division of Materials Science, U.S. Department of Energy. Authors at MIT and Tel Aviv University also acknowledge support by the US-Israel Binational Science Foundation. This work was also supported by the US-Japan Cooperative Neutron Scattering Program while that at Tohoku University was supported by a Grant-in-Aid for Scientific Research from the Japanese Ministry of Education, Science and Culture.

*Present address: Department of Physics, Princeton University, Princeton, NJ 08544.

¹J. G. Bednorz and K. A. Mueller, *Z. Phys. B* **64**, 189 (1986).

²For a review, see W. E. Pickett, H. Krakauer, R. E. Cohen, and D. J. Singh, *Science* **255**, 46 (1992).

³G. Shirane, R. J. Birgeneau, Y. Endoh, P. Gehring, M. A. Kastner, K. Kitazawa, H. Kojima, I. Tanaka, T. R. Thurston, and K. Yamada, *Phys. Rev. Lett.* **63**, 330 (1989); T. R. Thurston, R. J. Birgeneau, M. A. Kastner, N. W. Preyer, G. Shirane, Y. Fujii, K. Yamada, Y. Endoh, K. Kakurai, M. Matsuda, Y. Hidaka, and T. Murakami, *Phys. Rev. B* **40**, 4585 (1989); T. E. Mason, G. Aeppli, and H. A. Mook, *Phys. Rev. Lett.* **68**, 1414 (1992); T. R. Thurston, R. J. Birgeneau, Y. Endoh, P. M. Gehring, M. A. Kastner, H. Kojima, M. Matsuda, G. Shirane, I. Tanaka, and K. Yamada, *Phys. Rev. B* **46**, 9128 (1992).

⁴J. Rossat-Mignod, L. P. Regnault, C. Vettier, P. Bourges, P. Burlet, J. Bossy, J. Y. Henry, and G. Lapertot, *Physica C* **185-189**, 86 (1991); *Physica B* **180 & 181**, 383 (1992); J. M. Tranquada, P. M. Gehring, G. Shirane, M. Sato, and S. Shamoto, *Phys. Rev. B* **46**, 5561 (1992).

⁵Y. Endoh, K. Yamada, R. J. Birgeneau, D. R. Gabbe, H. P. Jenssen, M. A. Kastner, C. J. Peters, P. J. Picone, T. R. Thurston, J. M. Tranquada, G. Shirane, Y. Hidaka, M. Oda, Y. Enomoto, M. Suzuki, and T. Murakami, *Phys. Rev. B* **37**, 7443 (1988).

⁶K. Yamada, K. Kakurai, Y. Endoh, T. R. Thurston, M. A. Kastner, R. J. Birgeneau, G. Shirane, Y. Hidaka, and T. Murakami, *Phys. Rev. B* **40**, 4557 (1989).

⁷N. W. Preyer, R. J. Birgeneau, C. Y. Chen, D. R. Gabbe, H. P. Jenssen, M. A. Kastner, P. J. Picone, and T. Thio, *Phys. Rev. B* **42**, 11 563 (1989).

⁸C. Y. Chen, R. J. Birgeneau, M. A. Kastner, N. W. Preyer, and T. Thio, *Phys. Rev. B* **43**, 1 (1991).

⁹A. Aharony, R. J. Birgeneau, A. Coniglio, M. A. Kastner, and H. E. Stanley, *Phys. Rev. Lett.* **60**, 1330 (1988).

¹⁰B. J. Sternlieb, G. M. Luke, Y. J. Uemura, T. M. Riseman, J. H. Brewer, P. M. Gehring, K. Yamada, Y. Hidaka, T. Murakami, T. R. Thurston, and R. J. Birgeneau, *Phys. Rev. B* **41**, 8866 (1990).

¹¹B. Keimer, R. J. Birgeneau, A. Cassanho, Y. Endoh, R. W. Erwin, M. A. Kastner, and G. Shirane, *Phys. Rev. Lett.* **67**, 1930 (1991); R. J. Birgeneau, N. Belk, Y. Endoh, R. W. Erwin, M. A. Kastner, B. Keimer, and G. Shirane, *Physica B* **180 & 181**, 15 (1992).

¹²Y. Hidaka, Y. Enomoto, M. Suzuki, M. Oda, and T. Murakami, *J. Crystal Growth* **91**, 463 (1988).

¹³E. J. Opila, H. L. Tuller, B. J. Wuensch, and J. Maier, in *Symposium on Defects in Materials*, edited by P. D. Bristowe *et al.*, MRS Symposia Proceedings No. 209 (Materials Research Society, Pittsburgh, 1991).

¹⁴N. W. Preyer, M. A. Kastner, C. Y. Chen, R. J. Birgeneau, and Y. Hidaka, *Phys. Rev. B* **44**, 407 (1991).

¹⁵A. L. Efros and B. I. Shklovskii, *J. Phys. C* **8**, L49 (1975).

¹⁶T. Freltoft, G. Shirane, S. Mitsuda, J. P. Remeika, and A. S. Cooper, *Phys. Rev. B* **37**, 137 (1988).

¹⁷R. J. Birgeneau, J. Skalyo, and G. Shirane, *Phys. Rev. B* **3**, 1736 (1971).

¹⁸D. Vaknin, S. K. Sinha, D. E. Moncton, D. C. Johnston, J. M. Newsam, C. R. Safinya, and H. E. King, *Phys. Rev. Lett.* **58**, 2802 (1987).

¹⁹S. Chakravarty, B. I. Halperin, and D. R. Nelson, *Phys. Rev. B* **39**, 2344 (1989).

²⁰G. Aeppli, S. M. Hayden, H. A. Mook, Z. Fisk, S. W. Cheong, D. Rytz, J. P. Remeika, G. P. Espinosa, and A. S. Cooper, *Phys. Rev. Lett.* **62**, 2052 (1989).

²¹K. B. Lyons, P. A. Fleury, J. P. Remeika, A. S. Cooper, and T. J. Negrán, *Phys. Rev. B* **37**, 2353 (1988).

²²P. Hasenfratz and F. Niedermayer, *Phys. Lett. B* **268**, 231 (1991).

²³H. Q. Ding and M. Makivić, *Phys. Rev. B* **43**, 2662 (1991).

²⁴S. Tyc, B. I. Halperin, and S. Chakravarty, *Phys. Rev. Lett.*

- 62, 835 (1989).
- ²⁵P. Kopietz, Phys. Rev. Lett. **64**, 2587 (1990).
- ²⁶M. Matsuda, K. Yamada, H. Kadowaki, T. R. Thurston, Y. Endoh, Y. Hidaka, R. J. Birgeneau, M. A. Kastner, P. M. Gehring, A. H. Moudden, and G. Shirane, Phys. Rev. B **42**, 10 098 (1990).
- ²⁷B. Keimer, A. Aharony, A. Auerbach, R. J. Birgeneau, A. Cassanho, Y. Endoh, R. W. Erwin, M. A. Kastner, and G. Shirane, Phys. Rev. B **45**, 7430 (1992).
- ²⁸C. J. Peters, R. J. Birgeneau, M. A. Kastner, H. Yoshizawa, Y. Endoh, J. M. Tranquada, G. Shirane, Y. Hidaka, M. Oda, M. Suzuki, and T. Murakami, Phys. Rev. B **37**, 9761 (1988); T. Thio, C. Y. Chen, B. S. Freer, D. R. Gabbe, H. P. Jenssen, M. A. Kastner, P. J. Picone, and N. W. Preyer, *ibid.* **41**, 231 (1990).
- ²⁹B. Kelmer, R. J. Birgeneau, A. Cassanho, Y. Endoh, M. Greven, M. A. Kastner, and G. Shirane, Z. Phys. B (to be published).
- ³⁰M. Greven *et al.* (unpublished).
- ³¹S. W. Cheong, A. S. Cooper, L. W. Rupp, B. Batlogg, J. D. Thompson, and Z. Fisk, Phys. Rev. B **44**, 9739 (1991).
- ³²M. Matsuda, Y. Endoh, K. Yamada, H. Kojima, I. Tanaka, R. J. Birgeneau, M. A. Kastner, and G. Shirane, Phys. Rev. B **45**, 12 548 (1992).
- ³³J. M. Tranquada, G. Shirane, B. Keimer, S. Shamoto, and M. Sato, Phys. Rev. B **40**, 4503 (1989); J. Rossat-Mignod, L. P. Regnault, M. J. Jurgens, P. Burlet, J. Y. Henry, and G. Laperot, in *Dynamics of Magnetic Fluctuations in High-T_c Materials*, edited by G. Reiter, P. Horsh, and G. Psaltakis (Plenum, New York, 1990).
- ³⁴A. Muramatsu, Phys. Rev. Lett. **65**, 2909 (1990).
- ³⁵T. Yanagisawa, Phys. Rev. Lett. **68**, 1026 (1992).
- ³⁶T. Moriya, Y. Takahashi, and K. Ueda, J. Phys. Soc. Jpn. **59**, 2905 (1990).
- ³⁷A. J. Millis, H. Monien, and D. Pines, Phys. Rev. B **42**, 167 (1990).
- ³⁸R. J. Birgeneau, D. R. Gabbe, H. P. Jenssen, M. A. Kastner, P. J. Picone, T. R. Thurston, G. Shirane, Y. Endoh, M. Sato, K. Yamada, Y. Hidaka, M. Oda, Y. Enomoto, M. Suzuki, and T. Murakami, Phys. Rev. B **38**, 6614 (1988).
- ³⁹R. J. Gooding and A. Mailhot, Phys. Rev. B **44**, 11 852 (1991).
- ⁴⁰R. J. Birgeneau, R. A. Cowley, G. Shirane, J. A. Tarvin, and H. J. Guggenheim, Phys. Rev. B **21**, 317 (1980).
- ⁴¹I. Affleck and J. B. Marston, Phys. Rev. B **37**, 3774 (1988); J. B. Marston and I. Affleck, *ibid.* **39**, 11 538 (1989).
- ⁴²D. Poilblanc, E. Gagliano, S. Bacci, and E. Dagotto, Phys. Rev. B **43**, 10 979 (1991).
- ⁴³S. M. Hayden, G. Aeppli, H. Mook, D. Rytz, M. F. Hundley, and Z. Fisk, Phys. Rev. Lett. **66**, 801 (1990).
- ⁴⁴We thank H. Monien for pointing this out to us.
- ⁴⁵R. A. Cowley, R. J. Birgeneau, G. Shirane, and H. Yoshizawa, Phys. Scr. **T13**, 212 (1986).
- ⁴⁶L. P. Regnault, J. P. Boucher, J. Rossat-Mignod, J. Bouillot, R. Pynn, J. Y. Henry, and J. P. Renard, Physica B **136**, 329 (1986).
- ⁴⁷F. G. Mertens, A. R. Bishop, G. M. Wysin, and C. Kawabata, Phys. Rev. B **39**, 9162 (1989).
- ⁴⁸N. Bulut, D. Hone, D. J. Scalapino, and N. E. Bickers, Phys. Rev. Lett. **64**, 2723 (1990).
- ⁴⁹J. P. Lu, Q. Si, J. H. Kim, and K. Levin, Physica C **179**, 191 (1991); Q. Si, Y. Zha, K. Levin, J. P. Lu, and J. H. Kim (unpublished).
- ⁵⁰A. Virosztek and J. Ruvalds, Phys. Rev. B **42**, 4064 (1990).
- ⁵¹C. M. Varma, P. B. Littlewood, S. Schmitt-Rink, E. Abrahams, and A. E. Ruckenstein, Phys. Rev. Lett. **63**, 1996 (1989).
- ⁵²Y. Endoh, K. Yamada, K. Kakurai, M. Matsuda, N. Nakajima, R. J. Birgeneau, M. A. Kastner, B. Keimer, G. Shirane, and T. R. Thurston, Physica B **174**, 330 (1991).
- ⁵³R. J. Birgeneau, R. W. Erwin, P. M. Gehring, M. A. Kastner, B. Keimer, M. Sato, S. Shamoto, G. Shirane, and J. M. Tranquada, Z. Phys. B **87**, 15 (1992).
- ⁵⁴T. Imai, K. Yoshimura, T. Uemura, H. Yasuoka, and K. Kosuge, J. Phys. Soc. Jpn. **59**, 3846 (1990); S. E. Barrett, D. J. Durand, C. H. Pennington, C. P. Slichter, T. A. Friedman, J. P. Rice, and D. M. Ginsberg, Phys. Rev. B **41**, 6283 (1990); M. Takigawa, A. P. Reyes, P. C. Hammel, J. D. Thompson, R. H. Heffner, Z. Fisk, and K. C. Ott, *ibid.* **43**, 247 (1991).
- ⁵⁵T. Moriya and Y. Takahashi, J. Phys. Soc. Jpn. **60**, 776 (1991).
- ⁵⁶Z. Schlesinger, R. T. Collins, F. Holtzberg, C. Feild, S. H. Blanton, U. Welp, G. W. Crabtree, Y. Fang, and J. Z. Liu, Phys. Rev. Lett. **65**, 801 (1990).
- ⁵⁷S. Uchida, T. Ido, H. Takagi, T. Arima, Y. Tokura, and S. Tajima, Phys. Rev. B **43**, 7942 (1991).